TURBULENT SOLUTIONS OF EQUATIONS OF FLUID MOTION[*]

Robert G. Deissler
National Aeronautics and Space Administration
Lewis Research Center
Cleveland, Ohio 44135

Some turbulent solutions of the unaveraged Navier-Stokes equations (equations of fluid motion) are reviewed. Those equations are solved numerically in order to study the nonlinear physics of incompressible turbulent flow. Initial three-dimensional cosine velocity fluctuations and periodic boundary conditions are used in most of the work considered. The three components of the mean-square velocity fluctuations are initially equal for the conditions chosen. The resulting solutions show characteristics of turbulence, such as the linear and nonlinear excitation of small-scale fluctuations. For the stronger fluctuations the initially nonrandom flow develops into an apparently random turbulence. Thus randomness or turbulence can arise as a consequence of the structure of the Navier-Stokes equations. The cases considered include turbulence that is statistically homogeneous or inhomogeneous and isotropic or anisotropic. A mean shear is present in some cases. A statistically steady-state turbulence is obtained by using a spatially periodic body force. Various turbulence processes, including the transfer of energy between eddy sizes and between directional components and the production, dissipation, and spatial diffusion of turbulence, are considered. It is concluded that the physical processes occurring in turbulence can be profitably studied numerically.

I. INTRODUCTION

Nearly all of the flows occurring in nature, as well as those that are manmade, are turbulent. For instance, the boundary between a column of rising smoke and the surrounding atmosphere is generally irregular and contains a range of scales of motion, indicating the presence of turbulence. The atmosphere itself is usually turbulent, as shown by the irregular appearance of many of the clouds present in it. Jets, wakes, astrophysical flows, and flows over surfaces are commonly turbulent, as is the region downstream of a grid in a wind tunnel or downstream of a waterfall. In general, turbulent flows are the rule and laminar flows the exception.

Because of the importance and challenge of the turbulence problem a great deal of research has been done over the past century. Basic ideas have been set forth, for instance, in papers by Reynolds (1883, 1895), Taylor (1921, 1935), von Karman (1937a, 1937b), and Heisenberg (1948). That work, together with more recent research, is discussed in books by Batchelor (1953), Hinze (1975), Frost and Moulden (1977), and others.

In spite of considerable research activity there is no general deductive theory of high-Reynolds-number (strong) turbulence. (Reynolds number is defined as the product of a velocity and a length divided by the kinematic viscosity of the fluid. It is a measure of the ratio of inertial to viscous effects.) Most of the analytical theories depend on a closure assumption for

---

[*]Also published in Reviews of Modern Physics, vol. 56, no. 1, part I, April 1984.

a hierarchy of averaged equations.[1] This immediately calls into question the appropriateness of referring to the analytical theories as deductive, except at low Reynolds numbers or in the final stage of decay, where nonlinear effects are small (Batchelor, 1953; Deissler, 1977).

One way in which a closure assumption can be avoided is by closure by specification of sufficient random initial conditions (Deissler, 1979). That method can successfully predict turbulence decay, and in the sense that the evolution of all initially specified quantities can be calculated, gives a complete solution. To use it, however, the initial conditions must be fully turbulent, and a large amount of initial data is required to satisfactorily specify the initial turbulence. The method does not seem capable of extension to some cases of turbulence maintained by mean gradients, where the effect of initial conditions may eventually become negligible (e.g., in fully developed turbulent pipe flow).

In view of the foregoing comments it seems desirable to consider numerical solutions of the unaveraged Navier-Stokes equations that display features of turbulence. Numerical methods and computers can be considered as tools for the solution of equations, just as can Fourier transforms and series expansions. It might be pointed out that it is more appropriate to refer to a numerical solution of the unaveraged equations as deductive than it is to so refer to most of the analytical theories, which are based on averaged equations and require closure assumptions. Moreover, most of the analytical theories are so complicated that a large amount of numerical work is required to obtain results from them. Attempts to obtain analytical solutions of the unaveraged equations have not been successful, mostly because of the nonlinearity of those equations. Herring (1973) mentions that the simplest turbulence theory is just the Navier-Stokes equations. Since most turbulence calculations are numerical anyway, no insight is lost by considering direct integration of the Navier-Stokes equations forward in time, starting from some suitable initial data.

Numerical solution (or numerical simulation) has sometimes been called experiment. It seems, at least to this writer, that there is an important difference between numerical solution and experiment as generally practiced. The former uses directly, and attempts to solve, a given set of constitutive equations, in this case the Navier-Stokes equations. The latter ordinarily does not, although both methods may arrive at the same result if the constitutive equations are congruous with the portion of nature to which they are applied. In general, it appears that experiment works directly with nature, whereas numerical solution works with a set of constitutive equations that should represent at least a portion of nature.

Several numerical solutions of the unaveraged equations have appeared that use a spectrum of random initial fluctuations (e.g., Orszag and Patterson, 1972; Clark et al., 1979; Rogallo, 1981; and Feiereisen et al., 1982). These studies, which appear to demonstrate the feasibility of carrying out turbulent solutions with present-day computing equipment, represent major advances.

---

[1] The hierarchy of correlation (averaged) equations obtained from the unaveraged Navier-Stokes equations is unclosed because of the nonlinearity of the latter. That is, there are more unknowns than equations, so that a closure assumption is required to obtain a solution.

Because of the difficulty of specifying realistic turbulent initial con-
ditions (experimentally or analytically), it may be more appropriate to ini-
tially specify a simple regular fluctuation with a single length scale (as
actually occurs downstream of a grid in a wind tunnel). This should be better
for studying the development of small-scale fluctuations (and of turbulence in
general) than would a spectrum of initial fluctuations, since for the latter,
small-scale fluctuations are already present in the initial flow. Moreover,
much higher Reynolds number flows can be calculated with a given numerical grid
when a single length scale is initially present, at least for early and moder-
ate times. Taylor and Green (1937) and others (e.g., Deissler, 1970a;
Van Dyke, 1975; Corrsin and Kollman, 1977; and Deissler and Rosenbaum, 1973)
have used a perturbation series to calculate the nonlinear development of
higher harmonics from lower ones, but the calculations could not be carried
very far in time. In these analyses the directional components of the initial
fluctuation intensity were not equal. Orszag and Fateman (Orszag, 1977a) have
recently used Taylor and Green's initial conditions and obtained a numerical
solution for higher Reynolds numbers and longer times. The inviscid (infinite
Reynolds number) case was investigated in some detail by Betchov and Szewczyk
(1978).

The present review considers the nonlinear physics of turbulence numeri-
cally. Although the initial conditions used herein are nonrandom, the flow at
higher Reynolds numbers breaks up into an apparently random turbulence. Unlike
the problem of Taylor and Green all three of the directional components of the
mean-square velocity fluctuations are equal at the initial time. In the
absence of mean shear they are also equal at later times. Taylor and Green's
directional components, on the other hand, do not approach equality, even at
long times (Orszag, 1977a).

To study the processes in turbulence, first some background on the basic
fluid flow and turbulence equations is given in section II and on numerical
methods and solutions in section III. Four cases of turbulence are then con-
sidered, starting in section IV with the simplest one, in which mean gradients
are absent (Deissler, 1981a). In this case no energy sources are present and
the turbulence decays freely. (By contrast the presence of mean gradients
would imply energy sources in the flow.) Here (in section IV) one can study
viscous dissipation and the nonlinear transfer of energy between wave numbers
or eddy sizes, as well as the randomization of the flow. Next, in section V a
uniform mean shear is applied to study turbulence production and maintenance,
and the linear and nonlinear transfer of energy between wave numbers and
between directional components (Deissler, 1981c). The transfer of energy
between wave numbers (both linear and nonlinear) is manifested by the creation
of small-scale structure in the turbulence. Then, in section VI, the spatial
diffusion of the inhomogeneous turbulence in a developing shear layer is con-
sidered (Deissler, 1982). Finally, by using a spatially periodic body force a
turbulence that is statistically steady state at long times is studied in sec-
tion VII. The first three of these cases have also been studied, but with a
spectrum of random initial fluctuations and in some cases with an assumption
for the small eddies, in Orszag and Patterson (1972), Clark et al. (1979),
Rogallo (1981), Shannan et al. (1975), and Cain et al. (1981). Here we will
confine ourselves to the development of turbulence from nonrandom initial
conditions with a single length scale.

One of the problems in the numerical study of turbulence is that of accu-
racy, because of the small scale of some of the turbulent eddies. As the

Reynolds number (strength) of the turbulence or the time increases, smaller eddies are generated. No matter how small the numerical mesh size, one can always pick a Reynolds number or time large enough that the results will be quantitatively inaccurate. One way of improving the accuracy is by extrapolation to zero mesh size, as will be done here. The effectiveness of that procedure depends to some extent on the accuracy of the unextrapolated solution. If the solution has to be extrapolated too far, the results may not be accurate. Another popular method (not used here) is to model eddies smaller than the grid spacing (subgrid modeling) (e.g., Smagorinsky, et al., 1963; Deardorff, 1970; Clark et al., 1979; and Ferziger, 1977). This method requires an empirical input, although not as great a one as that for full modeling of the averaged equations. One might think of subgrid modeling as a useful crutch that can be phased out as numerical resolution improves. However, when it is used, it is sometimes difficult to tell which effects come from the equations of motion and which result from the subgrid modeling. Siggia (1981) has recently considered the converse problem; he made a numerical study of the small-scale eddies in which he modeled the larger ones.

Here we are mainly concerned with physical processes and trends, rather than with highly accurate numerical results (possibly unattainable at very high Reynolds numbers). Of course some degree of accuracy is necessary; otherwise we will not even be able to calculate trends. As the numerical mesh size decreases, quantitative differences in the results might be obtained. It is to be hoped, however, that the results will not be qualitatively different. Results to date indicate that to be the case.[2]

Other relevant review articles are given by Orszag (1977b), Schumann, et al. (1980), Eckman (1981), and Ott (1981).

II. BASIC EQUATIONS AND CONCEPTS

A. The Unaveraged Equations

Turbulent flows of a great many liquids and gases obey the Navier-Stokes equations. Those equations assume that the fluid is Newtonian (stress proportional to strain rate) and that it can be considered a continuum. The latter

---

[2]The attainment of accurate quantitative results appears to be a question of improvement of computers and of numerical methods. If state-of-the-art numerical methods and computers are used, good quantitative as well as qualitative results can already be obtained, at least for low and moderate Reynolds numbers. Orszag and Patera (1981) (as well as Moin and Kim (1982) using subgrid modeling) made significant numerical calculations of the velocity profile in the wall region of fully developed turbulent channel flow. The results agreed reasonably well with experiment, showing a wall transition region and a fully turbulent region in which the velocity varies as the logarithm of distance from the wall. The advent of high-speed computers and efficient numerical algorithms may be making possible for the first time the use of the Navier-Stokes equations in the solution of a wide range of realistic (turbulent) fluid-flow problems.

is usually a good assumption because in most cases intermolecular lengths are much smaller than the smallest significant turbulent eddies.

1. Equations in terms of instantaneous quantities

The Navier-Stokes and continuity equations for constant fluid properties (including incompressibility)[3,4] can be written as (e.g., Batchelor, 1967; or Deissler, 1976)

$$\frac{\partial \tilde{u}_i}{\partial t} = - \frac{\partial (\tilde{u}_i \tilde{u}_k)}{\partial x_k} - \frac{1}{\rho} \frac{\partial \tilde{p}}{\partial x_i} + v \frac{\partial^2 \tilde{u}_i}{\partial x_k \partial x_k} \tag{1}$$

and

$$\frac{\partial \tilde{u}_k}{\partial x_k} = 0 \tag{2}$$

The subscripts can take on the values 1, 2, and 3, and a repeated subscript in a term indicates a summation, with the subscript successively taking on the values 1, 2, and 3. The quantity $\tilde{u}_i$ is an instantaneous velocity component, x_i is a space coordinate, t is the time, ρ is the density, v the kinematic viscosity, and $\tilde{p}$ is the instantaneous pressure. Equations (1) and (2) are, respectively, statements of the conservation of momentum and of mass. In order to obtain an explicit equation for the pressure, we take the divergence of equation (1) and apply the continuity equation (2) to get

$$\frac{1}{\rho} \frac{\partial^2 \tilde{p}}{\partial x_\ell \partial x_\ell} = - \frac{\partial^2 (\tilde{u}_\ell \tilde{u}_k)}{\partial x_\ell \partial x_k} \tag{3}$$

In the remainder of the paper it will usually be convenient to use equations (1) and (3) rather than (1) and (2). Equations (1) (i = 1, 2, 3) and (3) constitute a set of four equations in the four unknowns u_i and p. Since they are for instantaneous velocities and pressures, they should apply to turbulent as well as to laminar flows, subject to the restrictions mentioned at the beginning of this section. The Navier-Stokes equations have been known for more than a century, but their use in turbulent flows, other than in a schematic sense, has been restricted by a lack of ability to obtain solutions. Now, with advances in computers and numerical methods the situation appears somewhat brighter.

---

[3]The continuity equation is sometimes included in the Navier-Stokes equations.

[4]Most turbulence studies have been carried out for constant properties, for simplicity. That flow is realistic if the turbulence velocities are reasonably low compared with the velocity of sound, and if temperature gradients are not large.

The fundamental turbulence problem is an initial-value problem. That is, given initial values for the u_i as functions of position, a value for ν, and suitable boundary conditions, equations (1) and (3) should be sufficient for calculating the u_i and p/ρ as functions of time and position. The initial and boundary conditions used herein are specified in section III.

To interpret the terms in equation (1), it is convenient to multiply it through by ρ and by the stationary volume element $dx_1\, dx_2\, dx_3$. Then the term on the left side of the equation is the time rate of change of momentum in the element $\rho u_i\, dx_1\, dx_2\, dx_3$. This rate of change is contributed to by the terms on the right side of the equation. The first term on the right side, a nonlinear inertia term, is the net rate of flow of momentum into the element through its faces. The next term, also nonlinear, is a pressure-force term and gives the net force acting on the element by virtue of the pressure gradient in the x_i direction. It is nonlinear because of the nonlinear source term on the right side of the Poisson equation for the pressure (eq. (3)). Finally, the last term in equation (1), a linear viscous-force term, gives the net force acting on the element in the x_i direction by virtue of the viscosity.

2. Equations in terms of mean and fluctuating components

Following Reynolds (1895) one can break the instantaneous velocities and pressure in equations (1) to (3) into mean and fluctuating (or turbulent) components; that is, set

$$\tilde{u}_i = U_i + u_i \tag{4}$$

and

$$\tilde{p} = P + p \tag{5}$$

where

$$\bar{u}_i = \bar{p} = 0 \tag{6}$$

$$U_i = \bar{\tilde{u}}_i \tag{7}$$

and

$$P = \bar{\tilde{p}} \tag{8}$$

The overbars designate averaged values.[5] Equation (2) becomes, on using equations (4), (6), and (7),

$$\frac{\partial u_k}{\partial x_k} = \frac{\partial U_k}{\partial x_k} = 0 \tag{9}$$

which shows that both the fluctuating and mean velocity components obey continuity. Equations (1) and (3) become, on using equations (4) to (9), taking averages, and subtracting the averaged equations from the unaveraged ones,

$$\frac{\partial u_i}{\partial t} = -\frac{\partial}{\partial x_k}(u_i u_k) - \frac{1}{\rho}\frac{\partial p}{\partial x_i} + \nu\frac{\partial^2 u_i}{\partial x_k \partial x_k} - u_k\frac{\partial U_i}{\partial x_k} - U_k\frac{\partial u_i}{\partial x_k} + \frac{\partial}{\partial x_k}\overline{u_i u_k} \qquad (10)$$

$$\frac{1}{\rho}\frac{\partial^2 p}{\partial x_\ell \partial x_\ell} = -\frac{\partial^2(u_k u_\ell)}{\partial x_k \partial x_\ell} - 2\frac{\partial u_k}{\partial x_\ell}\frac{\partial U_\ell}{\partial x_k} + \frac{\partial^2 \overline{u_k u_\ell}}{\partial x_k \partial x_\ell} \qquad (11)$$

Equations (10) and (11) will be used to study the processes in turbulence, but not for computational purposes (except in linearized cases). The first four terms of equation (10) and the first two of equation (11) look like the terms in equations (1) and (3), although their meanings are exactly the same only if $U_i = P = 0$ (eqs. (4) and (5)). The first three terms on the right side of equation (10), which contribute to $\partial u_i/\partial t$, can still be interpreted as an inertia-force (or turbulence self-interaction) term, a pressure-force term, and a viscous-force term. The remaining terms are, respectively, a turbulence production term, a mean-flow convection term, and a mean-turbulent-stress term, which appears when the turbulence is statistically inhomogeneous (when mean turbulence quantities such as $\overline{u_i u_k}$ are functions of position). (The reasons calling the production and convection terms as such will perhaps become clearer when the equivalent terms in the averaged equations (eqs. (14) and (15)) are discussed.) It will be seen that when the mean velocity gradient is not zero, the term $-U_k\,\partial u_i/\partial x_k$ generates a small-scale structure in the turbulence by vortex stretching. The nonlinear self-interaction term $-\partial(u_i u_k)/\partial x_k$ also produces a small-scale structure and in addition produces randomization of the flow. These effects will be considered in sections IV to VI. The Poisson equation for the pressure fluctuation (eq. (11)) has three source terms: a nonlinear term, a mean-gradient term, and a mean-turbulent-stress term, which appears when the turbulence is inhomogeneous.

We have defined an inhomogeneous turbulence as one in which averaged turbulence quantities are functions of position. Thus, a homogeneous turbulence is one in which averaged turbulence quantities are not functions of position. For instance, in homogenous turbulence

---

[5]For the most general flows the average is usually an ensemble average over a large number of macroscopically identical flows (i.e., mean quantities, but not fluctuating quantities, are the same in all the flows). In most cases, however, statistical uniformity or stationarity with respect to one or more coordinates, or with respect to time, obtains. Then, the average is taken with respect to the one or more coordinates or with respect to time. According to the ergodic theorem those averages are the same as the ensemble average if the flow is turbulent. In section V (uniform mean shear) three-dimensional spatial averages are used, even when the periodic boundary conditions introduce some local inhomogeneity into the fluctuations. Those averages still have meaning since their values are independent of the position of the boundaries of the cycle over which the averages are taken.

$$\overline{u_i u_j} \neq \overline{u_i u_j} \; (x_\ell)$$

$$\overline{u_i u_j u_k} \neq \overline{u_i u_j u_k} \; (x_\ell)$$

and

$$\overline{p \; \partial u_i / \partial x_j} \neq \overline{p \; \partial u_i / \partial x_j} \; (x_\ell)$$

Similar statements apply to other averaged turbulence quantities in a homogenous turbulence.

B. Averaged Equations

Although the averaged equations will not be solved numerically because they do not form a closed set, they are useful for studying the processes in turbulence.

1. Equations for mean flow

First consider the equations obtained by averaging each term of equations (1) and (3) and using equations (4) to (9).[5] This gives

$$\rho \frac{\partial U_i}{\partial t} = -\rho U_k \frac{\partial U_i}{\partial x_k} - \frac{\partial P}{\partial x_i} + \frac{\partial}{\partial x_k} \left(\rho \nu \frac{\partial U_i}{\partial x_k} - \rho \overline{u_i u_k} \right) \tag{12}$$

and

$$\frac{\partial^2 P}{\partial x_\ell \, \partial x_\ell} = - \rho \frac{\partial}{\partial x_\ell} \left(U_k \frac{\partial U_\ell}{\partial x_k} \right) - \rho \frac{\partial^2 \overline{u_\ell u_k}}{\partial x_\ell \, \partial x_k} \tag{13}$$

These equations look like equations (1) and (3) with instantaneous values replaced by average values, but with the important difference that an extra

term involving the quantity $\overline{u_i u_j}$ now appears in each of the equations. These terms arise from the nonlinear velocity terms in equations (1) and (3) and are a manifestation of the closure problem of turbulence[1]. If those terms were absent, equations (12) and (13) could be solved, and turbulent flows would be no more difficult to calculate than laminar ones. Note that terms in equations (12) and (13) that contain lower-case letters (other than x's) are turbulent terms.

The form of equation (12) suggests that the quantity $-\rho \overline{u_i u_k}$ augments the viscous stress $\rho \nu \partial U_i / \partial x_k$. Since it involves the fluctuating or turbulent velocity components u_i and u_k, we interpret it as a turbulent or

Reynolds stress. For instance $-\rho \overline{u_1 u_2}$ will, in the presence of a mean-velocity gradient $\partial U_1 / \partial x_2$, act like a shear stress on an x_1-x_3 plane. In the presence of $\partial U_1 / \partial x_2$, u_1 will more likely be negative than positive when u_2

is positive, so that $\overline{u_1 u_2}$ will have a nonzero negative value. The quantity $-\overline{\rho u_1 u_2}$ can be compared with a viscous shear stress obtained in the kinetic theory of gases, where u_1 and u_2 are now molecular, rather than macroscopic velocity components. Similarly $\overline{\rho u_1^2}$ will act like a normal stress on an x_2-x_3 plane (similar to a normal stress or pressure obtained in kinetic theory, where u_1 is again taken to be a molecular velocity component).

2. One-point correlation equations

a. Construction of equations

We can construct equations for the undetermined quantities $\overline{u_i u_j}$ in equations (12) and (13) from the evolution equation for u_i (eq. (10)) and a similar equation for the component u_j:

$$\frac{\partial u_i}{\partial t} = -\frac{\partial}{\partial x_k}(u_j u_k) - \frac{1}{\rho}\frac{\partial p}{\partial x_j} + \nu\frac{\partial^2 u_i}{\partial x_k \partial x_k} - u_k\frac{\partial U_i}{\partial x_k} - U_k\frac{\partial u_i}{\partial x_k} + \frac{\partial}{\partial x_k}\overline{u_j u_k}$$

Multiply equation (10) by u_j and the preceding equation for u_j by u_i, add the two equations, and average.[5] This gives, using continuity (eq. (9)),

$$\frac{\partial}{\partial t}\overline{u_i u_j} = -\left(\overline{u_j u_k}\frac{\partial U_i}{\partial x_k} + \overline{u_i u_k}\frac{\partial U_j}{\partial x_k}\right) - U_k\frac{\partial}{\partial x_k}\overline{u_i u_j}$$

$$-\frac{\partial}{\partial x_k}\overline{u_i u_j u_k} - \frac{1}{\rho}\left(\frac{\partial}{\partial x_i}\overline{p u_j} + \frac{\partial}{\partial x_j}\overline{p u_i}\right) + \nu\frac{\partial^2 \overline{u_i u_j}}{\partial x_\ell \partial x_\ell}$$

$$+\frac{1}{\rho}\left(\overline{p\frac{\partial u_j}{\partial x_i}} + \overline{p\frac{\partial u_i}{\partial x_j}}\right) - 2\nu\overline{\frac{\partial u_i}{\partial x_\ell}\frac{\partial u_j}{\partial x_\ell}} \qquad (14)$$

Setting $i = j$ and using continuity, we get, for the rate of change of the kinetic energy per unit mass,

$$\frac{\partial}{\partial t}\left(\frac{\overline{u_i u_i}}{2}\right) = -\overline{u_i u_k}\frac{\partial U_i}{\partial x_k} - U_k\frac{\partial}{\partial x_k}\left(\frac{\overline{u_i u_i}}{2}\right) - \frac{\partial}{\partial x_k}\left(\overline{\frac{u_i u_i}{2} u_k}\right)$$

$$-\frac{1}{\rho}\frac{\partial}{\partial x_k}\left(\overline{p u_k}\right) + \nu\frac{\partial^2 (\overline{u_i u_i}/2)}{\partial x_\ell \partial x_\ell} - \nu\overline{\frac{\partial u_i}{\partial x_\ell}\frac{\partial u_i}{\partial x_\ell}} \qquad (15)$$

As in equations (12) and (13), quantities in equations (14) and (15) that contain lower-case letters (other than x's) are turbulent quantities.

The one-point correlation equation (eq. (14)) gives an expression for the rate of change of $\overline{u_i u_j}$ that might be used in conjunction with equations (12) and (13). But the situation with respect to closure is now worse than it was before. Whereas without equation (14) we only had to determine $\overline{u_i u_j}$, with it we have to determine quantities like $\overline{u_i u_j u_k}$, $\overline{p u_j}$, $\overline{p\, \partial u_j / \partial x_i}$, and $\overline{(\partial u_i / \partial x_\ell)(\partial u_j / \partial x_\ell)}$. We might use equation (11) to obtain the pressure correlations, but that would only introduce more unknowns. However, equations (14) and (15) are useful for studying the processes in turbulence in that most of the terms have clear physical meanings. Moreover, we will be able to calculate terms in those equations from our numerical solutions.

b. Physical interpretation of terms

As in the case of equation (1) it is helpful, for purposes of interpretation, to multiply the terms in equations (14) and (15) through by ρ and by a volume element $dx_1\, dx_2\, dx_3$. Then the term on the left side of equation (14) or (15) gives the time rate of change of $\rho \overline{u_i u_j}$, or of the kinetic energy $\rho \overline{u_i u_i}/2$, within the element. This rate of change is contributed to by the terms on the right side of the equations. The first of those terms is equal to the net work done on the element by turbulent stresses acting in conjunction with mean-velocity gradients. It is therefore called a turbulence production term; it equals the rate of production of $\rho \overline{u_i u_j}$ or of $\rho \overline{u_i u_i}/2$ within the volume element by work done on the element. A somewhat abbreviated interpretation suggested by the form of the term, which is often given, is that it represents work done on the turbulent stress $\rho \overline{u_i u_i}$ by the mean-velocity gradient.

The next term in each of the equations describes the convection or net flow of turbulence or turbulent energy into a volume element by the mean velocity U_k. It moves the turbulence bodily, rather than doing work on it by deforming it, as in the case of the production term. It vanishes when either U_k is zero (no mean flow) or when the turbulence is homogenous $(\overline{u_i u_j} \neq \overline{u_i u_j} (x_k))$. In the latter case there is no accumulation of turbulence within a volume element, even with a mean flow.

The next three terms in equation (14) and in equation (15) also vanish for homogeneous turbulence. Since they do not contain the mean velocity, they do not convect or move the turbulence bodily. Therefore we interpret them as diffusion terms, which diffuse net turbulence from one part of the turbulent field to another by virtue of its inhomogeneity. The pressure-velocity-gradient terms in equation (14) drop out of the contracted equation (15) because of continuity (eq. (9)). Therefore, they contribute nothing to the rate of change of the total energy $\overline{u_i u_i}/2$, but they can distribute the energy among the three directional components $\overline{u_{(i)}^2}/2$ (no sum on i). The last term in equations (14) and (15) is the viscous dissipation term, which dissipates turbulence by the presence of fluctuating velocity gradients.

3. Two-point correlation and spectral equations

To consider the transfer of turbulence between eddy sizes or wave numbers (spectral transfer), we must obtain two-point correlation equations. Terms related to that process do not appear in the single-point equations ((14) and (15)). To obtain two-point equations, we use in addition to equations (10) and (11), written at the point P, the following equations written at the point P':

$$\frac{\partial u_j'}{\partial t} = -\frac{\partial}{\partial x_k'}(u_j'u_k') - \frac{1}{\rho}\frac{\partial p'}{\partial x_j'} + \nu\frac{\partial^2 u_j'}{\partial x_k'\partial x_k'} - u_k'\frac{\partial U_j'}{\partial x_k'} - U_k'\frac{\partial u_j'}{\partial x_k'} + \frac{\partial}{\partial x_k'}\overline{u_j'u_k'} \qquad (16)$$

and

$$\frac{1}{\rho}\frac{\partial^2 p'}{\partial x_\ell'\partial x_\ell'} = -\frac{\partial^2(u_k'u_\ell')}{\partial x_k'\partial x_\ell'} - 2\frac{\partial u_k'}{\partial x_\ell'}\frac{\partial U_\ell'}{\partial x_k'} + \frac{\partial^2\overline{u_k'u_\ell'}}{\partial x_k'\partial x_\ell'} \qquad (17)$$

Multiplying equation (10) by u_j' and equation (16) by u_i, adding, taking averages,[5] and using equation (16) and the fact that quantities at one point are independent of the position of the other point result in

$$\frac{\partial}{\partial t}\overline{u_iu_j'} = -\overline{u_ku_j'}\frac{\partial U_i}{\partial x_k} - \overline{u_iu_k'}\frac{\partial U_j'}{\partial x_k'} - U_k\frac{\partial}{\partial x_k}\overline{u_iu_j'} - U_k'\frac{\partial}{\partial x_k'}\overline{u_iu_j'} - \frac{\partial}{\partial x_k}\overline{u_iu_ku_j'}$$

$$- \frac{\partial}{\partial x_k'}\overline{u_iu_j'u_k'} - \frac{1}{\rho}\left(\frac{\partial}{\partial x_i}\overline{pu_j'} + \frac{\partial}{\partial x_j'}\overline{u_ip'}\right) + \nu\left(\frac{\partial^2\overline{u_iu_j'}}{\partial x_k\partial x_k} + \frac{\partial^2\overline{u_iu_j'}}{\partial x_k'\partial x_k'}\right) \qquad (18)$$

To simplify the equations, the turbulence will be considered homogeneous (correlations independent of x_i). (See Hinze (1975) or Deissler (1961) for inhomogeneous equations.) Then the two-point correlations (e.g., $\overline{u_iu_j'}$) will be functions only of $r_i \equiv x_i' - x_i$, so that $\partial/\partial x_i = -\partial/\partial r_i$ and $\partial/\partial x_i' = \partial/\partial r_i$. In addition, homogeneity requires that $\partial U_i/\partial x_j$ be a constant, so that $\partial U_i/\partial x_j = \partial U_i'/\partial x_j'$ and $U_k' - U_k = r_i\,\partial U_k/\partial x_i$. (If $\partial U_i/\partial x_j$ were a function of x_j, we could not remove all x_i' dependency from eq. (18).) Equation (18) becomes

$$\frac{\partial}{\partial t}\overline{u_iu_j'} = -\overline{u_ku_j'}\frac{\partial U_i}{\partial x_k} - \overline{u_iu_k'}\frac{\partial U_j}{\partial x_k} - \frac{1}{\rho}\left(\frac{\partial}{\partial r_j}\overline{u_ip'} - \frac{\partial}{\partial r_i}\overline{pu_j'}\right)$$

$$+ 2\nu\frac{\partial^2\overline{u_iu_j'}}{\partial r_k\partial r_k} - \frac{\partial U_k}{\partial x_\ell}r_\ell\frac{\partial\overline{u_iu_j'}}{\partial r_k} - \frac{\partial}{\partial r_k}\left(\overline{u_iu_j'u_k'} - \overline{u_iu_ku_j'}\right) \qquad (19)$$

The equations for the pressure-velocity correlations obtained from equations (11) and (17) are, for homogeneous turbulence,

105

$$\frac{1}{\rho} \frac{\partial^2 \overline{u_1 p'}}{\partial r_\ell \partial r_\ell} = -2 \frac{\partial \overline{u_1 u_k'}}{\partial r_\ell} \frac{\partial U_\ell}{\partial x_k} - \frac{\partial^2 \overline{u_1 u_\ell' u_k'}}{\partial r_\ell \partial r_k} \tag{20}$$

$$\frac{1}{\rho} \frac{\partial^2 \overline{p u_j'}}{\partial r_\ell \partial r_\ell} = 2 \frac{\partial \overline{u_\ell u_j'}}{\partial r_k} \frac{\partial U_k}{\partial x_\ell} - \frac{\partial^2 \overline{u_\ell u_k u_j'}}{\partial r_\ell \partial r_k} \tag{21}$$

a. Interpretation of terms

The terms on the right side of the Poisson equations (eqs. (20) and (21)) are source terms associated with the mean velocity and with triple correlations arising from the nonlinear velocity terms in equations (11) and (17). The right side of the two-point equation (eq. (19)) contains, as in the case of the single-point equation (eq. (14)), turbulence production, directional distribution (pressure-velocity), and viscous terms. There are no diffusion terms in equation (19) since the turbulence is homogeneous. The last two terms in that equation are new terms that do not have counterparts in the single-point equations. To interpret them, we convert equation (19) to spectral form by taking its Fourier transform. Thus, define the following three-dimensional Fourier transforms:

$$\overline{u_1 u_j'} (\vec{r}) = \int_{-\infty}^{\infty} \varphi_{ij}(\vec{\kappa}) e^{i\vec{\kappa} \cdot \vec{r}} \, d\vec{\kappa} \tag{22}$$

$$- \frac{\partial}{\partial r_j} \overline{u_1 p'} + \frac{\partial}{\partial r_i} \overline{p u_j'} = \int_{-\infty}^{\infty} \Pi_{ij}(\vec{\kappa}) e^{i\vec{\kappa} \cdot \vec{r}} \, d\vec{\kappa} \tag{23}$$

$$- \frac{\partial U_k}{\partial x_\ell} r_\ell \frac{\partial \overline{u_1 u_j'}}{\partial r_k} = \int_{-\infty}^{\infty} T'_{ij}(\vec{\kappa}) e^{i\vec{\kappa} \cdot \vec{r}} \, d\vec{\kappa} \tag{24}$$

and

$$- \frac{\partial}{\partial r_k} \overline{u_1 u_j' u_k'} - \overline{u_1 u_k u_j'} = \int_{-\infty}^{\infty} T_{ij}(\vec{\kappa}) e^{i\vec{\kappa} \cdot \vec{r}} \, d\vec{\kappa} \tag{25}$$

where φ_{ij}, Π_{ij}, T'_{ij}, and T_{ij} are, respectively, Fourier transforms of the quantities on the left sides of the defining equations (eqs. (22) to (25)), $\vec{\kappa}$ is a wave-number vector, and $d\vec{\kappa} = d\kappa_1 d\kappa_2 d\kappa_3$. Physical interpretations of the Fourier transforms defined by equations (22) to (25) follow. Equation (19) becomes, on taking its Fourier transform,

$$\frac{\partial}{\partial t} \varphi_{ij} = - \varphi_{kj} \frac{\partial U_i}{\partial x_k} - \varphi_{ik} \frac{\partial U_j}{\partial x_k} + \frac{1}{\rho} \Pi_{ij}(\vec{\kappa}) - 2v\vec{\kappa}^2 \varphi_{ij} + T'_{ij} + T_{ij} \tag{26}$$

If we let $\vec{r} = 0$ in equation (22), we have

$$\overline{u_i u_j} = \int_{-\infty}^{\infty} \varphi_{ij} \, d\vec{\kappa} \qquad (27)$$

so that we can interpret φ_{ij} as a spectral component of $\overline{u_i u_j}$. As in equation (19), terms on the right side of equation (26) can be interpreted as production, directional distribution, and viscous dissipation terms. They contribute to the rate of change of a spectral component φ_{ij} of $\overline{u_i u_j}$.

To interpret the term T'_{ij} in equation (26), we let $\vec{r} = 0$ in equation (24). This gives

$$0 = \int_{-\infty}^{\infty} T'_{ij} \, d\vec{\kappa} \qquad (28)$$

Thus, T'_{ij} gives zero total contribution to the rate of change of $\overline{u_i u_j}$. But it can distribute, or transfer between wave numbers or eddy sizes, spectral contributions φ_{ij} to $\overline{u_i u_j}$. So T'_{ij}, which is proportional to $\partial U_k / \partial x_\ell$, is interpreted as a mean-gradient spectral transfer term (Deissler, 1961). The term $-r_\ell (\partial \overline{u_i u_j} / \partial r_k) \, \partial U_k / \partial x_\ell$ in equation (19) is therefore the Fourier transform of a mean-gradient spectral transfer term.

To interpret the last term in equation (26), we use equation (25), where we note that $\partial / \partial r_k = \partial / \partial x'_k = -\partial / \partial x_k$, that quantities at one point are independent of the position of the other point, and that continuity (eq. (9)) holds. Equation (25) becomes

$$\int_{-\infty}^{\infty} T_{ij} \, e^{i\vec{\kappa} \cdot \vec{r}} \, d\vec{\kappa} = -\overline{\frac{\partial}{\partial x'_k} u_i u'_j u'_k} - \overline{\frac{\partial}{\partial x_k} u_i u_k u'_j}$$

$$= -\overline{u_i u'_k \frac{\partial u'_j}{\partial x'_k}} - \overline{u'_j \frac{\partial u_i u_k}{\partial x_k}} \qquad (29)$$

If we let $\vec{r} = 0$, equation (29) becomes

$$\int_{-\infty}^{\infty} T_{ij} \, d\vec{\kappa} = -\frac{\partial}{\partial x_k} \overline{u_i u_j u_k} = 0 \qquad (30)$$

since we have assumed homogeneity of the turbulence. Thus, as in the case of T'_{ij}, T_{ij} contributes nothing to the rate of change of $\overline{u_i u_j}$. It can, however, transfer spectral components of $\overline{u_i u_j}$ from one part of wave-number space to another. So we interpret T_{ij} as a spectral transfer term associated with turbulence self-interaction (as opposed to interaction between

turbulence and mean gradients). The term $-(\partial/\partial r_k)(\overline{u_i u_j' u_k'} - \overline{u_i u_k u_j'})$ in equation (19) is therefore the Fourier transform of a self-interaction spectral transfer term. Although the turbulence has been assumed to be homogeneous for interpreting T_{ij} and T_{ij}' as transfer terms, it has been shown that similar interpretations apply when the turbulence is inhomogeneous (Deissler, 1981b).[6]

The transfer of turbulence from one part of wave-number space to another, or from one eddy size to another, produces a wide range of scales of motion in most turbulent flows as illustrated by the numerical solutions in sections IV and V (e.g., figs. 2(c), 8, and 24). The state of affairs is neatly summarized in a nonmathematical way by a poem written long before equations (26), (28), or (30) was known (Richardson, 1922):

> Big whirls have little whirls,
> Which feed on their velocity;
> And little whirls have lesser whirls,
> And so on to viscosity.

4. Vorticity and dissipation

For homogeneous turbulence one can obtain a relation between the viscous dissipation term in equation (15) or (19) ($i = j$) and the vorticity or swirl in the turbulence. The dimensionless vorticity $\vec{\omega}$ is defined as the curl of $\vec{u}$:

$$\vec{\omega}(\vec{x}) = \vec{\nabla} \times \vec{u}(\vec{x}) \tag{31}$$

or

$$\omega_i = \varepsilon_{ijk} \frac{\partial u_k}{\partial x_j} \tag{32}$$

where ε_{ijk} is the alternating tensor.[7] Then

$$\overline{\omega_k \omega_k} = \varepsilon_{ijk} \varepsilon_{pmk} \overline{\frac{\partial u_i}{\partial x_j} \frac{\partial u_\ell}{\partial x_m}} = (\delta_{ip}\delta_{jm} - \delta_{im}\delta_{jp}) \overline{\frac{\partial u_i}{\partial x_j} \frac{\partial u_\ell}{\partial x_m}} = \overline{\frac{\partial u_i}{\partial x_j} \frac{\partial u_i}{\partial x_j}} - \overline{\frac{\partial u_i}{\partial x_j} \frac{\partial u_j}{\partial x_i}} \tag{33}$$

But, because

$$\frac{\partial u_i}{\partial x_j} = 0 \tag{34}$$

---

[6]The fact that terms related to T_{ij} or T_{ij}' do not appear in the one-point eq. (14) for inhomogeneous turbulence indicates that T_{ij} and T_{ij}' do not contribute to $\partial \overline{u_i u_j}/\partial t$. Thus, even for inhomogeneous turbulence they can only transfer turbulence from one part of wave-number space to another.

$$\overline{\frac{\partial u_i}{\partial x_j} \frac{\partial u_j}{\partial x_i}} = \frac{\partial^2 \overline{u_i u_j}}{\partial x_i \, \partial x_j} = 0 \tag{35}$$

for homogeneous turbulence. Equation (33) then becomes

$$\overline{\omega_k \omega_k} \equiv \overline{\omega^2} = \overline{\frac{\partial u_i}{\partial x_j} \frac{\partial u_i}{\partial x_j}} \equiv \frac{\varepsilon}{\upsilon} \tag{36}$$

Thus, for homogeneous turbulence the mean-square vorticity is just the rate of viscous dissipation ε of turbulent energy divided by the kinematic viscosity (eq. (15)). So the more intense the swirl in the turbulence, the faster it dissipates.

From a closure standpoint we are somewhat better off with the two-point equations (eqs. (19) to (21)) than we were with the single-point equation (eq. (14)), since we no longer have to model terms like $\overline{p \, \partial u_j / \partial x_i}$ and $\overline{(\partial u_i / \partial x_\ell)(\partial u_j / \partial x_\ell)}$. However, we still have to evaluate triple-correlation terms unless the turbulence is very weak or unless the interaction between the turbulence and the mean flow is large compared with the turbulence self-interaction.

5. Remarks

We shall not discuss here the many schemes that have been proposed for closing the averaged equations considered in this section. Instead, we will avoid the closure problem by obtaining numerical solutions of the unaveraged equations (eqs. (1) and (3)). The importance of the averaged equations is enhanced by these numerical solutions; by using the solutions of the unaveraged equations, terms in the averaged equations that represent various physical processes in the turbulence can be calculated. Thus, the averaged equations appear to be necessary, or at the least very convenient, for the physical interpretation of the numerical results.

III. NUMERICAL SOLUTIONS AND METHODS

A. Initial conditions

For most of the numerical solutions considered here, the initial velocity fluctuation is assumed to be given by

$$u_i = \sum_{n=1}^{3} a_i^n \cos \vec{q}^n \cdot \vec{x} \tag{37}$$

Then, from equation (4)

---

[7]$\varepsilon_{ijk} = 0$ when i, j, and k are not all different. When the subscripts are all different, $\varepsilon_{ijk} = +1$ when they are in cyclic order and -1 when they are in acyclic order.

$$\tilde{u}_i = \sum_{n=1}^{3} a_i^n \cos \vec{q}^n \cdot \vec{x} + U_i \tag{38}$$

The quantity a_i^n is an initial velocity amplitude or Fourier coefficient of the velocity fluctuation, $\vec{q}^n$ is an initial wave-number vector, and U_i is an initial mean-velocity component. To satisfy the continuity conditions (eqs. (2) and (9)), we set

$$a_i^n q_i^n = 0 \tag{39}$$

For the present work let

$$a_i^1 = k(2, \pm 1, 1), \quad a_i^2 = k(1, \pm 2, 1), \quad a_i^3 = k(1, \pm 1, 2) \tag{40}$$

$$q_i^1 = (-1, \pm 1, 1)/x_0, \quad q_i^2 = (1, \mp 1, 1)/x_0, \quad q_i^3 = (1, \pm 1, -1)/x_0$$

where k has the dimensions of a velocity and determines the intensity of the initial velocity fluctuation. The quantity x_0 is the length scale of the initial velocity fluctuation. The quantities k and x_0, together with the kinematic viscosity v and equation (40) then determine the initial Reynolds number $\overline{u_0^2}^{1/2} x_0/v$, since the square of equation (37), averaged over a period, gives $\overline{u_0^2}$. In addition to satisfying the continuity equation (eq. (39)), equations (37) and (40) give

$$\overline{u_1^2} = \overline{u_2^2} = \overline{u_3^2} = \overline{u_0^2} \tag{41}$$

at the initial time.[8] Thus, equations (37) or (38) and (40) give a particularly simple initial condition in that we need specify only one component of the mean-square velocity fluctuation. Moreover, for no mean shear they give an isotropic turbulence at later times, as will be seen. Note that it is necessary to have at least three terms in the summation in equation (37) or (38) to satisfy equation (41). We do not specify an initial condition for the pressure because it is determined by equation (3) and the initial velocities.

B. Numerical grid and boundary conditions

To carry out numerical solutions subject to the initial condition given by equations (37) or (38) and (40), we use a stationary cubical grid with a maximum of 32^3 points and with faces at $x_i^* = x_i/x_0 = 0$ and 2π. For boundary conditions we assume periodicity for the fluctuating quantities. That is, let

$$(u_i)_{x_j^* = 2\pi + b_j^*} = (u_i)_{x_j^* = b_j^*} \tag{42}$$

and

$$P_{x_j^* = 2\pi + b_j^*} = P_{x_j^* = b_j^*} \tag{43}$$

for $b_j^* \ll 2\pi$, where $b_j^* = b_j/x_0$, $x_j^* = x_j/x_0$, and b_j is a variable length.

By using equations (4) and (5) these become

$$(\tilde{u}_i)_{x_j^* = 2\pi + b_j^*} = (\tilde{u}_i)_{x_j^* = b_j^*} + (U_i)_{x_j^* = 2\pi + b_j^*} - (U_i)_{x_j^* = b_j^*} \tag{44}$$

and

$$\tilde{p}_{x_j^* = 2\pi + b_j^*} = \tilde{p}_{x_j^* = b_j^*} + P_{x_j^* = 2\pi + b_j^*} - P_{x_j^* = b_j^*} \tag{45}$$

In the present work we assume also that P, given by equation (13), is periodic, so that

$$P_{x_j^* = 2\pi + b_j^*} = P_{x_j^* = b_j^*} \tag{46}$$

and equation (45) becomes

$$\tilde{p}_{x_j^* = 2\pi + b_j^*} = \tilde{p}_{x_j^* = b_j^*} \tag{47}$$

These equations are used to calculate numerical derivatives at the boundaries of the computational grid.

C. Numerical solutions

In carrying out the numerical solutions, we have a choice of solving a set of equations containing u_i, p, U_i, and P (eqs. (10) to (13)), or one containing $\tilde{u}_i$ and $\tilde{p}$ (eqs. (1) and (3)). The latter set, which is much simpler, is generally used here.[9] That is, we solve equations (1) and (3) subject to initial condition (38) and boundary conditions (44) and (47).

The spatial- and time-differencing schemes (which numerically conserve momentum and energy) are essentially those used by Clark et al. (1979). For the spatial derivatives in equations (1) and (3) we use centered fourth-order difference expressions (e.g., McCormick and Salvadore, 1964). For instance, the fourth-order difference expression used for $\partial \tilde{u}_i / \partial x_k$ is

---

[8]The first three terms of eq. (41) apply at all times when there are no mean gradients in the flow.

$$\left(\frac{\partial \tilde{u}_1}{\partial x_k}\right)_n = \frac{1}{12\,\Delta x_k}\left[(\tilde{u}_1)_{n-2} - 8(\tilde{u}_1)_{n-1} + 8(\tilde{u}_1)_{n+1} - (\tilde{u}_1)_{n+2}\right]$$

where Δx_k is the grid-point spacing, and the subscripts n, $n + 1$, etc. refer to grid points in the x_k direction. Fourth-order difference expressions are often considered more efficient than the usual second-order ones (Orszag and Israeli, 1974). (Spectral methods devised by Orszag and associates are still more efficient but may be somewhat trickier to use.) Centered expressions (same number of points on both sides of n, see preceding expression) can be used both at interior grid points and at the boundaries of the grid; when n refers to a point on a boundary, values for $\tilde{u}_1$ outside of the grid, which are required for calculating the numerical derivatives at the boundary, are obtained from boundary condition (44).

For time differencing we use a predictor-corrector method with a second-order (leapfrog) predictor and a third-order (Adams-Moulton) corrector (Ceschino and Kuntzman, 1966). If m represents a time step, and $(R_1)_m$ the right side of equation (1), then at each grid point in space the second-order leapfrog predictor for $\tilde{u}_1$ at time step $m + 1$ is

$$(\tilde{u}_1)^{(1)}_{m+1} = (\tilde{u}_1)_{m-1} + 2\,\Delta t(R_1)_m$$

and the third-order Adams-Moulton corrector is

$$(\tilde{u}_1)^{(2)}_{m+1} = (\tilde{u}_1)_m + \frac{\Delta t}{12}\left[5(R_1)^{(1)}_{m+1} + 8(R_1)_m - (R_1)_{m-1}\right]$$

where Δt is the time increment. The quantity $(R_1)^{(1)}_{m+1}$ in the preceding corrector is calculated by using $(\tilde{u}_1)^{(1)}_{m+1}$ in the right side of equation (1), where $(\tilde{u}_1)^{(1)}_{m+1}$ is calculated from the leapfrog predictor. Note that the leapfrog method (so-called because it leaps over the time step m), although unstable for all Δt when used by itself for Navier-Stokes equations, is stable when used as a predictor.

The Poisson equation for the pressure (eq. (3)) is solved directly by a fast Fourier transform method. This method of solution was found to preserve continuity quite well ($\nabla \cdot \vec{u} \approx 0$) except near the ends of some of the runs for no mean gradients, where the solutions began to deteriorate. (Another indication of incipient solution deterioration near the ends of some of the runs for no mean gradients was that equation (41) was no longer accurately satisfied.[8])

---

[9]Dividing the velocities and pressures into mean and fluctuating components is evidently not advantageous from a computational standpoint except, possibly, in linearized cases.

Two known types of numerical instabilities can occur in the present solutions: a viscous instability connected with the first and last terms in equation (1), which occurs if $v \, \Delta t/(\Delta x_k)^2$ is too large; and a convective instability connected with the first and second terms (or the first and third terms through eq. (3)), which occurs if $u_i \, \Delta t/\Delta x_k$ is too large. In these criteria Δt, Δx_k, and u_i are, respectively, a time step, distance step, and velocity. Thus, a particular solution should be numerically stable if, for a given Δx_k, the time step is sufficiently small. Numerical stability is typically obtained when the solution varies smoothly from time step to time step, with no significant breaks in the slope from one step to the next. This is the case for all of the results given here.

For the present solution very good temporal resolution is obtained automatically when Δt is sufficiently small to give numerical stability. That temporal resolution is much better than the three-dimensional spatial resolution, which is more severely limited by the storage and power of the computer. However, as will be seen (fig. 19), sufficient spatial resolution is obtained to give reasonably accurate averaged results for times not excessively large. Some of the averaged results are extrapolated to zero spatial mesh size in an effort to obtain more accuracy. The fourth-order method of extrapolation (consistent with the fourth-order differencing used here) is given in Deissler (1981a, 1981c).

IV. HOMOGENEOUS FLUCTUATIONS AND TURBULENCE, NO MEAN FLOW

For this case ($U_i = \partial \overline{u_i u_k}/\partial x_k = 0$), equations (10) and (11) reduce to (1) and (3) without the ~'s over instantaneous quantities. We thus solve numerically

$$\frac{\partial u_i}{\partial t} = - \frac{\partial(u_i u_k)}{\partial x_k} - \frac{1}{\rho}\frac{\partial p}{\partial x_i} + v \frac{\partial^2 u_i}{\partial x_k x_k} \tag{48}$$

and

$$\frac{1}{\rho}\frac{\partial^2 p}{\partial x_\ell \, \partial x_\ell} = - \frac{\partial^2(u_\ell u_k)}{\partial x_\ell x_k} \tag{49}$$

subject to initial conditions (37) and (40) and boundary conditions (42) and (43). In equation (40) for the coefficients in the initial conditions, we choose the first set of signs.

A. Dimensionless form of equations

For carrying out the numerical solutions and presenting the results in as general and compact a form as possible, we nondimensionalize equations (48) and (49) as

$$\frac{\partial u_i^*}{\partial t^*} = - \frac{\partial(u_i^* u_k^*)}{\partial x_k^*} - \frac{\partial p^*}{\partial x_i^*} + \frac{\partial^2 u_i^*}{\partial x_k^* \partial x_k^*} \tag{48a}$$

113

and

$$\frac{\partial^2 p^*}{\partial x_\ell^* \, \partial x_\ell^*} = - \frac{\partial^2 (u_\ell^* u_k^*)}{\partial x_\ell^* \, \partial x_k^*} \tag{49a}$$

where

$$u_i^* = \frac{x_0}{v} u_i, \quad t^* = \frac{v}{x_0^2} t$$

$$x_i^* = \frac{x_i}{x_0}, \quad p^* = \frac{x_0^2}{\rho v^2} p$$

and x_0 is the initial fluctuation length, which first appeared in equation (40). Note that all of the quantities have been nondimensionalized by x_0 and the kinematic viscosity v.

The initial and boundary conditions in equations (37), (40), (42), and (43) become in dimensionless form

$$u_i^* = \sum_{n=1}^{3} a_i^{n*} \cos \vec{q}^{n*} \cdot \vec{x}^* \tag{37a}$$

$$\left.\begin{array}{l} a_i^{1*} = k^*(2,\pm1,1), \; a_i^{2*} = k^*(1,\pm2,1), \; a_i^{3*} = k^*(1,\pm1,2) \\[2mm] q_i^{1*} = (-1,\pm1,1), \; q_i^{2*} = (1,\mp1,1), \; q_i^{3*} = (1,\pm1,-1) \end{array}\right\} \tag{40a}$$

$$(u_i^*)_{x_j^*=2\pi+b_j^*} = (u_i^*)_{x_j^*=b_j^*} \tag{42a}$$

and

$$p^*_{x_j^*=2\pi+b_j^*} = p^*_{x_j^*=b_j^*} \tag{43a}$$

where, in addition to the dimensionless quantities defined above,

$$a_i^{n*} = \frac{x_0}{v} a_i^n, \quad q_i^{n*} = x_0 q_i^n, \quad \text{and} \quad k^* = \frac{x_0}{v} k.$$

Note that k^* has the form of a Reynolds number, where x_0 is the length and k is the velocity. The initial Reynolds number appearing in the figures of this paper, $\left(\overline{u_0^2}\right)^{1/2} x_0/v$, where $\left(\overline{u_0^2}\right)^{1/2}$ is an initial root-mean-square velocity component, is obtained by choosing a value for k^* in equations (40a) and

114

space averaging u_1^{*2} over a period, by using equation (37a). The value of $\left(\overline{u_0^{*2}}\right)^{1/2} = \left(\overline{u_0^2}\right)^{1/2} x_0/\nu$ so obtained is also used in the ordinates of figures 1 and 2, where $u_1/\left(\overline{u_0^2}\right)^{1/2} = u_1^*/\left(\overline{u_0^{*2}}\right)^{1/2}$, and u^* is calculated from equations (48a) and (49a) (starting with initial values from eq. (37a)).

B. Development of random fluctuations

Figure 1 shows the calculated evolution of velocity fluctuations (normalized by the initial root-mean-square velocity) at two fixed points in space for the initial Reynolds number shown in the figure (no correction for discretization error). Since there is no input of energy, the fluctuating motion eventually decays to a state of rest. In spite of the nonrandom initial condition (eq. (37) or (37a)), the velocity fluctuations have the appearance of those for a random turbulence. It is important to point out that the fluctuations are not due to numerical instability since a large number of time steps (typically about 20) lie between changes of sign of du_i/dt. In connection with the high Reynolds number in figure 1 it might be pointed out that Betchov and Szewczyk (1978) obtained reasonable turbulent-like numerical results even for infinite Reynolds number for times not excessively large (see also Schumann et al., 1980).

1. Randomness as sensitivity to initial conditions

The dashed curves of $u_1/\left(\overline{u_0^2}\right)^{1/2}$ are for initial conditions perturbed approximately 0.1 percent. (The coefficients a_1^n and q_1^n given by eq. (40) are changed by 0.1 percent of their values.) The perturbed curves follow the unperturbed ones for a short time and then depart sharply. Thus, a very small perturbation of initial conditions causes a large change in the values of u_i (except near $t = 0$). On the other hand, the root-mean-square values of the velocities (spatially averaged) decrease smoothly and are unaffected by the perturbation of the initial conditions. All of these features are characteristic of turbulence. (The observed sensitivity of the instantaneous flow to small changes in initial conditions may have unfavorable implications for detailed long-term weather predictions (Lorenz, 1963).)

We note that the spatially averaged values in figure 1 follow approximately the decay law $\overline{u^2} \sim t^{-n}$, where $n \sim 2.5$. This lies between the value for n of 3.3 observed for turbulence downstream of a waterfall (Ling and Saad, 1977), and the value of 1.2 generally observed for turbulence generated by flow through a grid in a wind tunnel (Uberoi, 1963). The decay law is evidently very much dependent on the initial condition for the turbulence.

2. Effect of numerical mesh size on randomness

To get an idea of the effect of mesh size in the numerical grid on the apparent randomness of the velocity fluctuations, values of $u_1/\left(\overline{u_0^2}\right)^{1/2}$ at the center of the grid are plotted against t^* in figure 2 for three mesh sizes. All three of the curves have a random appearance. However, as the number of mesh points increases (as the mesh becomes finer), smaller scale

fluctuations are resolved and the randomness appears to be greater. This trend indicates that the observed randomness is not due to the use of too coarse a grid.

C. Further evidence for randomness and indications of isotropic turbulence

For turbulence the correlation between velocities at two times $\overline{u_1(t)u_1(t_0)}$ should go to zero as the separation of the times t and t_0 increases. Figure 3 shows that this occurs for the present high-Reynolds-number calculations. For true turbulence the correlation should probably decrease smoothly with time. This is nearly the case for the larger t_0 (fig. 3(b)). (t_0 is the time in the correlation coefficient in fig. 3 that remains fixed as the other (variable) time t increases.) At early times there is probably some nonrandom structure in the turbulence caused by the nonrandom initial conditions (fig. 3(a)).

As a further indication that the high-Reynolds-number flow breaks up into turbulence, we calculate the evolution of the cross correlation $\overline{u_1 u_2}$. Although $\overline{u_1^2} = \overline{u_2^2} = \overline{u_3^2}$ at all times,[8] the initial $\overline{u_1 u_2}$ given by equations (37) and (40) is not zero. However, figure 4 shows that because of the apparent randomization of the flow $\overline{u_1 u_2}$ goes to zero as time increases. The fluctuations in the curve at early times (as also in the curve of fig. 3(a)) are probably caused by nonrandom structure in the flow at early times.[10]

Figures 1 to 4, together with the fact that the three components $\overline{u_{(1)}^2}$ are equal, show that at later times we appear to get a reasonable approximation to isotropic turbulence, although the initial conditions are nonrandom.

One of the consequences of isotropy is that the cross correlations, say $\overline{u_1 u_2}$, are zero, as in figure 4 at later times. These calculations differ from others where turbulence was obtained by using random initial conditions.

Because the initial conditions for the present calculations are nonrandom, the turbulence must arise as a result of the structure of the Navier-Stokes equations. In particular the nonlinear terms play a crucial role. It is easy to verify that if nonlinear terms are neglected for the present case, equations (48), (49), (37), and (40) give

$$u_i = (u_i)_0 \, e^{-3t^*} \tag{50}$$

So if the equations are linear, the flow given by the nonrandom initial condition (37) remains nonrandom. The nonlinear terms must be present in equations (48) and (49) if the development of turbulence is to take place.

---

[10]All averaged values would be expected to vary smoothly only for highly random fluctuations.

Our calculations at lower Reynolds numbers give results that are less like turbulence. Thus, the fluctuations develop apparent randomness only at the higher Reynolds numbers.

Calculated values of velocity-derivative skewness factor for a high Reynolds number (fig. 5) also appear to be of reasonable magnitude when compared with experimental values for isotropic turbulence. Values of that quantity of the order of 0.4 have been obtained experimentally and have long been considered an indication of true moderately strong or strong isotropic turbulence. The falloff near the end of the curve may be due to a more laminar flow there, where fluctuation levels are lower. A longer period of agreement with experimental values is obtained by Clark et al. (1979), apparently because they used turbulent initial conditions, so that the turbulence was already partially developed at $t = 0$.

D. Origin of the randomness (strange behavior)

A question remains as to how the nonlinear terms in equations (48) and (49) produce the randomness observed in figures 1 to 4. Until recently, it was generally assumed that randomness in a turbulent flow is due to randomness in the initial conditions, to random external fluctuations, or to the presence of so many eddies or harmonic components (or of so many degrees of freedom) that the identity of the individual eddies is lost (Monin, 1978; Rabinovich, 1978). In the present results the first of these is absent. Concerning the second, roundoff errors might be considered a form of external fluctuations. However, when the calculations were repeated using double precision, so that roundoff errors were reduced by a factor of about 10^6, the mean-square velocities were practically unchanged. The instantaneous velocities were different, although still as random as before. Thus, the effect of a large decrease in roundoff errors is similar to the effect of a small perturbation of the initial conditions (fig. 1). Since roundoff errors do not affect the turbulence level or the randomness, they cannot be considered a major sustaining cause of the turbulence or randomness observed here, although they may in some cases affect the initial transition. In the present case the transition is so rapid that the effect appears to be small.

This leaves only the proliferation of eddies or harmonic components as a source of apparent randomness. That might well produce the randomness observed in figure 1, since the nonlinear production of harmonics tends to be explosive, particularly at high Reynolds numbers (each harmonic component interacts with every other one) (Deissler, 1970a). However, the randomness may be produced, at least partially, by strange attractors or, more properly, by analogous strange behavior (Eckmann, 1981; Ott, 1981). (We talk about analogous strange behavior here, rather than strange attractors, since, strictly speaking, strange attractors exist only for steady-state turbulence (section VII-A). Here, analogous strange behavior refers mainly to apparent randomness in flows where a large number of degrees of freedom or harmonic components are not a necessary ingredient and randomness occurs by a loss of hydrodynamic stability.) Lorenz (1963) and others (Monin, 1978; Rabinovich, 1978; Ruelle, 1976; Lanford, 1982) have shown that a system of nonlinear ordinary differential equations similar to the spatially differenced form of the Navier-Stokes equations used here, or to the spectral form of those equations (Orszag, 1977b), can develop an apparently random behavior in time as a result of the loss of

117

stability of the solutions.[11] In conjunction with this, regions appear in
the phase space of the system to which solutions are attracted. Randomness
arises in those regions, which are known as strange attractors, from a haphaz-
ard movement of the phase point among the neighborhoods of various critical
points in the phase space (steady-state points of unstable equilibrium where
$\partial u_i/\partial t = 0$). (The presence of critical (or fixed) points is not always con-
sidered a necessary ingredient of strange attractors, but randomness or sensi-
tivity to initial conditions is essential. However, the spatially differenced
and spectral forms of the Navier-Stokes equations do appear to have critical
points, as do the Lorenz equations.) Unlike randomization by proliferation of
harmonic components, randomization by strange behavior can occur either with a
few or with many degrees of freedom. In the present case both processes may be
important. At any rate, as mentioned earlier, the results show that the struc-
ture of the Navier-Stokes equations is such that apparently random or turbulent
solutions can arise from nonrandom initial conditions. With the results from
the low-order models, in which apparent randomness appears with as few as three
degrees of freedom (e.g., in the Lorenz equations), the turbulence observed to
be manufactured by the Navier-Stokes equations should perhaps not come as a
surprise.

The presence of strange behavior may be fortunate from a numerical stand-
point in that it should enable turbulent solutions that are qualitatively cor-
rect (at least insofar as they appear random in time) to be obtained with a
relatively coarse grid. The use of a fine three-dimensional grid, of course,
requires the use of a large amount of computer time.

Figure 6 shows a dimensionless velocity component u_1 plotted against
component u_2 (forming a plane in phase space) for one point in physical
space. Although the behavior here is much more complicated than that observed
for the low-order models that are usually used to observe strange attractors
or strange behavior (here there are not well-defined orbits around fixed crit-
ical points, possibly because there may be an almost infinite number of criti-
cal points), there are similarities. Both the present turbulent results and
those for the low-order models show trajectories consisting of loops and cusps,
with frequent changes in the sign of the curvature of the trajectory (e.g.,
Franceschini, 1983). (Note that the present turbulent results ultimately
decay, whereas the low-order models usually do not, since they contain forcing
terms.) Although there are large changes in the direction of the trajectory,
particularly in the regions of the cusps, the density of calculated points in
those regions is very high, so that the numerical results should be reasonably
accurate. Curves for u_i versus t (the numerical integrations are with
respect to t) are, in fact, smooth. Note that u_1 and u_2 start out equal
(on a 45° line) but that their equality is quickly destroyed when randomness
sets in.

---

[11]Results from the differenced or spectral forms of the Navier-Stokes
equations become arbitrarily close to those from the original equations as the
number of grid points or Fourier components increases (assuming convergence of
the numerical method). Theoretically, the Navier-Stokes equations correspond
to an infinite number of ordinary differential equations or to an infinite
number of degrees of freedom.

Randomization by strange behavior, or by a loss of hydrodynamic stability, almost certainly occurs in the present high-order turbulent results (high order here meaning many numerical grid points and thus many equations and degrees of freedom). This follows, first, from the fact that such randomness has been demonstrated to occur in low-order models (few equations and few degrees of freedom), such as that of Lorenz (1963) or Franceschini (1983), and second, from the fact that with the many more degrees of freedom present here than in the low-order models, many more critical points exist, and thus many more opportunities for randomization or loss of stability occur. Of course, because of the many degrees of freedom here, there will also be randomization by proliferation of harmonic components (so many harmonic components or eddies present that the identity of the individual eddies is lost and the flow appears random). The present large number of degrees of freedom encourages both types of randomness, and both very likely occur.

E. Evolution of mean quantities

In the results given so far, no correction for discretization error due to the finite numerical mesh size was applied. The primary purpose of the present work, of course, is to study the physics of turbulence rather than to obtain highly accurate results (possibly unattainable at very high Reynolds numbers). For low Reynolds numbers surprisingly good results for the decay can be obtained even with coarse grids (fig. 7). At higher Reynolds numbers the results, although less accurate, should still be qualitatively correct. Their accuracy can be improved by applying fourth-order extrapolations to zero numerical grid spacing (in consistency with the fourth-order numerical differencing used in the calculations (Deissler, 1981a)). This is done in lieu of subgrid modeling (making an assumption for the eddies smaller than the numerical grid spacing), e.g., Clark, et al., 1979. The method is related to subgrid modeling in that it assumes that the subgrid eddies are closely related to the calculated eddies but does not require the introduction of a subgrid eddy viscosity (which is, in effect, a kind of closure assumption). In all of the remaining results in this section the fourth-order discretization corrections are applied by extrapolating results for three mesh sizes to zero mesh size. However, the corrections are negligibly small except at the highest Reynolds number.

1. Mean-square velocity fluctuations

Figure 8 shows the calculated evolution of mean-square velocity fluctuations (spatially averaged) for a series of initial Reynolds numbers. As the Reynolds number increases (v and initial length scale x_0 held constant), the rate of decay of $\overline{u^2}$ increases sharply, as in experimental turbulent flows (Deissler, 1979). This can be attributed to the nonlinear excitation of small-scale turbulence-like fluctuations at the higher Reynolds numbers. The high shear stresses between the small eddies cause a rapid decay.

2. Microscales and nonlinear transfer of turbulence to smaller eddies

The development of the small-scale eddies is seen more clearly in figure 9, where the microscale λ, normalized by its initial value, is plotted against dimensionless time. The microscale is defined by

$$\overline{\frac{\partial u_i}{\partial x_\ell} \frac{\partial u_i}{\partial x_\ell}} \propto - \frac{\overline{u_i u_i}}{\lambda^2} \qquad (51)$$

For homogeneous turbulence and $U_i = 0$, λ can be calculated from equation (15) as

$$\lambda^2 \propto -v \frac{\overline{u_i u_i}}{\overline{du_i u_i}/dt} \qquad (52)$$

As the Reynolds number increases, the small-scale structure becomes finer. The microscale decreases until the fluctuation level (inertial effect) is low enough so that viscous forces prevent a further decrease. After λ decreases to a minimum, it begins to grow. (Results for coarser grids were not qualitatively different from these, but the minimums were somewhat higher.) The increase of λ at later times is due to the selective annihilation of eddies by viscosity, the small eddies being the first to decay. Thus, at large times only the big eddies remain. It is this period of increasing λ that is generally observed experimentally in grid-generated turbulence (turbulence observed downstream of a grid of wires or bars whose plane is normal to the flow in a wind tunnel). The increases of λ with time observed experimentally (Batchelor, 1953, fig. 7.2) are generally of the same order as those in figure 9 (doubling the time increases λ by a factor of about 1.5). The early period, in which λ decreases with time, is of interest as illustrative of inter-wave-number energy transfer. To generate the small-scale structure, turbulent energy must be transferred from big eddies to small ones.

For homogeneous turbulence the equation for the rate of change of turbulent kinetic energy (eq. (15)) reduces to

$$\frac{\partial}{\partial t} \left(\frac{\overline{u_i u_i}}{2} \right) = -v \overline{\frac{\partial u_i}{\partial x_\ell} \frac{\partial u_i}{\partial x_\ell}} \qquad (53)$$

That is, only viscous dissipation contributes to the rate of change of kinetic energy, there being no indication that nonlinear transfer of energy between scales of motion is taking place. There may seem to be a paradox here in view of the large transfer of energy to smaller eddies indicated in figure 9. This is as it should be, however, since energy transfer between wave numbers or scales of motion should not contribute to the rate of change of total energy. To consider inter-wave-number energy transfer, two-point equations must be used. Thus, equation (30) shows that the self-interaction transfer term $T_{ij}(\vec{\kappa})$ in the two-point spectral equation (eq. (26)) has the property that

$$\int_{-\infty}^{\infty} T_{ij}(\vec{\kappa}) \, d\vec{\kappa} = 0$$

as a spectral transfer term should. The quantity $\vec{\kappa}$ is the wave-number vector. The spectral transfer term $T_{ij}(\vec{\kappa})$, or its Fourier transform $-\partial(\overline{u_i u_j' u_k'} - \overline{u_i u_k u_j'})/\partial r_k$ in equation (19), is responsible for the generation of the small-scale structure in figure 9. Those terms come from the nonlinear term $-\partial(u_i u_k)/\partial x_k$ in the unaveraged equation (48). As mentioned earlier, the term $-\partial(u_i u_k)/\partial x_k$ produces randomization, as well as spectral energy transfer.

Although equation (30) shows that T_{ij} can transfer energy between wave numbers without contributing to the rate of change of total energy $\partial\overline{u_i u_j}/\partial t$, it says nothing about the direction of the transfer or how important it is. For that we need calculations such as those in figure 9, which show that significant energy is transferred to smaller eddies.[12] The energy transfer can be thought of as due to a breakup of big eddies into smaller ones or as a stretching of vortex filaments to smaller diameters. In spite of this transfer to smaller eddies, experimental results generally show a growth of scale (Batchelor, 1953, fig. 7.2). The reason is that those results are usually for the later period shown in figure 9, where, although energy is transferred to smaller eddies, the annihilation of small eddies by viscous action eventually wins out. The early period shown in figure 9, and in figure 2 of Taylor and Green (1937), is of particular interest in that the nonlinear transfer effects are truly dominant there; a sharp decrease in scale actually occurs as energy is transferred to smaller eddies.

3. Dissipation, vorticity generation, and pressure fluctuations

The energy dissipation term, the only term contributing to the rate of change of kinetic energy for homogeneous turbulence without mean gradients (eq. (53)) is plotted in figure 10. That is also the mean-square vorticity (eq. (36)), but the two are distinct physical entities. Although the curve for zero Reynolds number, where nonlinear effects are absent, decreases monotonically to zero, the curves for higher Reynolds numbers increase sharply for a while and then decrease. Thus, the nonlinear terms in the Navier-Stokes equations are very effective vorticity generators and greatly enhance the dissipation at short and moderate times. For long times they appear to have the opposite effect, evidently because the turbulence itself decays rapidly to zero. Nonlinear effects, although they do not appear explicitly in the evolution equation for $\overline{u_i u_i}$ (eq. (53)), thus alter greatly the evolution by altering the dissipation term.

---

[12] A direct numerical calculation of T_{ii} by Clark et al. (1979) for random initial conditions, and corresponding to the region of increasing λ in fig. 8, shows the same thing. Calculated values of T_{ii} are negative at small wave numbers (large eddies) and positive at large wave numbers (small eddies), so that energy is transferred from big eddies to smaller ones.

Figure 11 shows mean-square pressure fluctuations plotted against dimensionless time. The enhancement of the pressure fluctuations, although not as great as that of the vorticity or dissipation, again is due to nonlinear effects: in this case the nonlinear terms on the right side of the Poisson equation for the pressure cause the effect.

4. Further discussion and summary of the processes in isotropic turbulence

Nonlinear velocity and pressure terms do not appear in the evolution equation for $\overline{u_i u_i}$ (eq. (53)). But we can calculate root-mean-square values of the nonlinear terms in the instantaneous evolution equation (eq. (48)), as well as of the linear term. Three measures of the relative importance of inertial (nonlinear) and viscous effects are shown for a moderate Reynolds number in figure 12. The ratio of the nonlinear velocity term to the viscous term and the ratio of the pressure to the viscous term in equation (48), together with the microscale Reynolds number, are plotted against dimensionless time. The terms are space-averaged root-mean-square values. All of those measures show a variation from a rather inertial to a weak fluctuating flow. For instance, R_λ varies from about 90 to 0.7. This is a much greater variation than has been obtained experimentally for a single run. The curves for the term ratios lie somewhat below that for R_λ. They indicate that except at early times the nonlinear inertial effects associated with velocity and with pressure do not differ greatly.

The importance of both nonlinear velocity and pressure effects in figure 12 is somewhat paradoxical in view of equation (53), which says that neither contributes directly to $\partial \overline{u_i u_i}/\partial t$. The nonlinear velocity effects were already discussed in this section; it was pointed out that such effects should not appear in equation (53), since they only distribute energy in wave-number space and so do not directly alter the total energy. Although there is no nonlinear velocity term in equation (53), such a term appears in the two-point equation for $\partial \overline{u_i u_i'}/\partial t$. That equation, for the present case, is obtained from equation (19) as

$$\frac{\partial}{\partial t} \overline{u_i u_i'} = 2\nu \frac{\partial^2 \overline{u_i u_i'}}{\partial r_k \partial r_k} - \frac{\partial}{\partial r_k} (\overline{u_i u_i' u_k'} - \overline{u_i u_k u_i'}) = 3 \frac{\partial}{\partial t} \overline{u_i u_{(i)}'} \qquad (54)$$

where $\vec{r}$ is again the vector extending from the unprimed to the primed point, and the pressure terms drop out because of continuity. The last term, where the parenthesis indicates no sum on i, is a consequence of the isotropy of the turbulence. The equation for the rate of change of each component of $\overline{u_i u_i'}$ is contributed to by the nonlinear velocity term $-(\partial/\partial r_k)(\overline{u_i u_i' u_k'} - \overline{u_i u_k u_i'})$, but there is no contribution from the pressure. The strong effect of pressure shown in figure 12 must be contained in higher order equations in the hierarchy of averaged equations (moment equations) (Deissler, 1958 and 1960). Thus, although two-point averaged equations contain a nonlinear effect of velocity, we must consider higher order multipoint equations to obtain an effect of pressure. Terms in the unaveraged equations shown in figure 12 (averaged over space after the solution has been obtained) include effects of all orders.

(Effects contained in the numerical results may, however, be limited by the fineness of the numerical grid.)

Although there is a strong effect of pressure in figure 12, the physical significance of that effect is somewhat elusive in contrast to the effects of viscous dissipation and spectral energy transfer. If the turbulence is aniso-tropic, a clear effect of pressure fluctuations is that they transfer net energy among directional components (eqs. (14) and (15) and the discussion following those equations). That is discussed in the following section. If, in addition, the turbulence is inhomogeneous, pressure can produce a net spa-tial diffusion of energy (eq. (15)). Those are evidently the only physical effects of pressure fluctuations (at least that we know about). Thus, if the turbulence is homogeneous and isotropic, as it is here, it seems reasonable to attribute the observed pressure effects in the unaveraged equations to those processes. Even though there is no net interdirectional transfer or spatial diffusion of turbulence when the turbulence is isotropic, those processes can still be instantaneously or locally operative. They could, for instance, cause a diffusion of tagged particles. According to figure 12, they have a signifi-cant indirect effect on the evolution of the turbulence.

From the findings of the present section we conclude that the following processes occur in isotropic turbulence: nonlinear randomization by prolifer-ation of harmonic components or by strange behavior, nonlinear spectral trans-fer of turbulence among wave numbers or eddy sizes (mainly to smaller eddies), spatial diffusion and transfer of turbulence among directional components by pressure forces (with zero net diffusion and transfer into each component), generation of vorticity or swirl, and dissipation of turbulence into heat by viscous action.[13] From this description the life of isotropic turbulence appears interesting and includes many aspects.

V. UNIFORMLY SHEARED FLUCTUATIONS AND TURBULENCE

In the preceding section the evolution of nonrandom initial fluctuations into isotropic turbulence was examined numerically. The nonlinear transfer of energy to smaller scales of motion, the zero net (but not zero) spatial diffu-sion and transfer of energy among directional components, the generation of vorticity or swirl, and viscous dissipation were studied.

Another important process is the production of turbulence by a mean shear. Most turbulent flows, both those occurring in nature and those which are man-made, are in fact shear flows, where the turbulence is produced and maintained by the shear. Because of the added complexity the nonlinear problem of turbu-lent shear flow is even more difficult than that of isotropic turbulence. So it is not surprising that little progress has been made in obtaining an ana-lytical solution from first principles. An attempt to obtain a numerical solution would seem to be in order.

Conceptually, the simplest turbulent shear flow, although certainly not the simplest to produce experimentally (Champagne, et al., 1970), is one in which the turbulence is uniformly sheared. At least two significant numerical studies of that type of turbulence have recently been made (Rogallo, 1981;

[13]According to eq. (36), the vorticity and the dissipation are numerically the same, but they are physically distinct.

Shaanan, et al., 1975). In both of those studies random initial conditions with a range of eddy sizes were used.

In the spirit of the preceding section the present numerical study of uniformly sheared turbulence starts with simple determinate initial conditions that possess a single length scale. As in the preceding section, we can in this way study how the turbulence develops from nonturbulent initial conditions. Again, much higher Reynolds number flows can be calculated with a given numerical grid when a single length scale is initially present, at least for short and moderate times.

Several interesting results that could not be obtained in the previous work on turbulent shear flow are obtained here. One of the significant findings is that the structure of the turbulence produced in the presence of a strong shear is much finer than that produced in its absence.

A. Initial and boundary conditions

In carrying out numerical solutions for uniformly sheared turbulence the instantaneous equations (1) and (3), subject to initial condition (38) and boundary conditions (44) and (47) are used. Since we are considering a uniform shear, we let

$$U_i = \delta_{i1} \frac{dU_1}{dx_2} x_2 \tag{55}$$

in the initial condition (38) and

$$(U_i)_{x_j^* = 2\pi + b_j^*} - (U_i)_{x_j^* = b_j^*} = \delta_{i1} \delta_{j2} 2\pi \frac{dU_1}{dx_2} \tag{56}$$

in boundary condition (44). For the coefficients in equation (38) we use equation (40), where we choose the first set of signs. Equations (1) and (3) are written in terms of the total velocity $\tilde{u}_i$, but we can calculate the fluctuating component u_i from equation (4). It should be emphasized that we consider here not a sawtooth type of mean velocity profile, but a continuous profile in which the mean-velocity gradient is uniform at all points. Even with a uniform mean velocity gradient, some local inhomogeneity is introduced into the fluctuations by the periodic boundary conditions. We will not concern ourselves with that inhomogeneity, however, since we can still calculate products of velocities and pressures averaged over a three-dimensional period. Those values are independent of the position of the boundaries of the cycle. Note that for constant uniform mean-velocity gradient and mean pressure the last terms in equations (10) and (11) are zero even though the fluctuations may be inhomogeneous (eqs. (12) and (13)).

The u_2 component of the velocity fluctuation (in the direction of the mean-velocity gradient) is crucial in maintaining the turbulence against the dissipation (Deissler, 1970b and 1972). Therefore, when for brevity only one component of the velocity fluctuation is discussed, that component is chosen as u_2. More will be said about the maintenance of the turbulence later.

B. Development of random fluctuations

Figure 13 shows the evolution of $u_2 / \left(\overline{u_0^2} \right)^{1/2}$ at a fixed point in space for a high Reynolds number, as calculated from the full nonlinear equations. As in the preceding section asterisks on quantities indicate that they have been nondimensionalized by using the initial length scale x_0 and the kinematic viscosity v. Thus $t^* = (v/x_0^2)t$, $x_1^* = x_1/x_0$, and $(dU_1/dx_2)^* = (x_0^2/v)dU_1/dx_2$. Again the velocity fluctuations have the appearance of those for a random turbulence in spite of the nonrandom initial condition (eq. (37)). The dashed curves for $u_2 / \left(\overline{u_0^2} \right)^{1/2}$ are again for initial conditions perturbed approximately 0.1 percent. The perturbed curves at first follow the unperturbed ones but eventually depart sharply. Although the the curves in figures 13(a) and (b) differ considerably in appearance, the perturbed curves in the two figures take about the same length of time to break away from the unperturbed ones. A very small perturbation of initial conditions causes a large change in the values of u_2 except at small times. On the other hand, the root-mean-square values of the velocities change smoothly with time and are unaffected by the perturbation of the initial conditions. These features are characteristic of turbulence. (Although the root-mean-square curve in fig. 13(a) appears almost horizontal, it eventually goes smoothly to zero when extended.)

C. Shear-related small-scale structure

A striking feature of the curves for $u_2 / \left(\overline{u_0^2} \right)^{1/2}$ in figure 13 is the small scale structure exhibited for sheared turbulence (fig. 13(b)) when compared with the structure for no shear (fig. 13(a)). This shear-related small-scale structure is produced by the term $-U_k \, \partial u_i/\partial x_k$ in equation (10) which, for uniform shear, is $-(dU_1/dx_2)x_2 \, \partial u_i/\partial x_1$. Equation (10) becomes, for a constant uniform mean-velocity gradient and a uniform mean pressure,

$$
\frac{\partial u_1}{\partial t} = -\delta_{11} \frac{dU_1}{dx_2} u_2 - \frac{dU_1}{dx_2} x_2 \frac{\partial u_1}{\partial x_1} - \frac{\partial}{\partial x_k} (u_1 u_k) - \frac{1}{\rho} \frac{\partial p}{\partial x_1} + v \frac{\partial^2 u_1}{\partial x_k \partial x_k} \tag{57}
$$

where equation (12) is used. Note that equation (57) is obtained without the assumption of homogeneity. From the term $-(dU_1/dx_2)x_2 \, \partial u_i/\partial x_1$ in equation (57), we get the term

$$
- \frac{\partial U_k}{\partial x_\ell} r_\ell \frac{\partial \overline{u_i u_j'}}{\partial r_k} = - \frac{dU_1}{dx_2} r_2 \frac{\partial \overline{u_i u_j'}}{\partial r_1} \tag{58}
$$

in the two-point correlation equation (19). For periodic boundary conditions x_i dependency is not present in equations (19) and (58) because averages are taken over a three-dimensional period with r_i held constant. This is so even though the periodic boundary conditions may introduce some local inhomogeneities. If we take the Fourier transform of that term, we obtain the mean-gradient transfer term T_{ij}' in the spectral equation (26). Its effect in transferring energy to small-scale components is similar to that of the non-linear transfer term T_{ij} in equation (26) (the Fourier transform of the

125

triple correlation term in eq. (19)). The production of small-scale structure by the shear might be thought of as due to stretching of the random vortex lines in the turbulence by the mean gradient or to stretching of mean vortex lines by the turbulence.

Although we first discussed a mean-gradient transfer term more than two decades ago (Deissler, 1961), the present results give the first graphic demonstration of the effectiveness of that term in producing a small-scale structure in turbulence. Since that is a linear effect (when the mean gradient is given), we can study it either by the full nonlinear solutions already considered in figure 13 (which contain linear as well as nonlinear effects) or by linearized solutions.

Equation (11) becomes, for uniform shear and uniform mean pressure,

$$\frac{\partial^2 p}{\partial x_\ell \, \partial x_\ell} = - \frac{\partial^2 (u_k u_\ell)}{\partial x_k \, \partial x_\ell} - 2 \frac{\partial u_2}{\partial x_1} \frac{\partial U_1}{\partial x_2} \tag{59}$$

where equation (13) is used. As in the case of equation (57), equation (59) is obtained without the assumption of homogeneity.

D. Some linearized solutions and comparison with nonlinear solutions

Equations (57) and (59) are linearized by neglecting the terms $-\partial(u_1 u_k)/\partial x_k$ and $-\partial^2(u_k u_\ell)/\partial x_k \partial x_\ell$. The numerical solution, with initial and (periodic) boundary conditions given by equations (37), (40), (42), and (43), then proceeds as in the nonlinear case.

We can obtain an analytical solution for unbounded linearized fluctuations by using unbounded three-dimensional Fourier transforms (Deissler, 1961). The solution does not satisfy constant periodic boundary conditions. Instead of working with the averaged equations (Deissler, 1961), it is instructive to work with the unaveraged ones and use the initial condition given by equation (37). In this case the Fourier transforms must be generalized functions (a series of delta functions), but the method of solution is the same as that in the earlier work. Equation (57) for u_2 and equation (59), when linearized, are independent of u_1 and u_3. The solution obtained by using the initial condition (37) is

$$u_2 = \sum_{n=1}^{3} U_2^n \cos\left(\vec{q}^n \cdot \vec{x} - a q_1^n t x_2\right) \tag{60}$$

$$p = \sum_{n=1}^{3} P^n \sin\left(\vec{q}^n \cdot \vec{x} - a q_1^n t x_2\right) \tag{61}$$

where

$$U_2^n = \frac{a_2^n q^{n^2}}{q^{n^2} - 2aq_1^n q_2^n t + a^2 q_1^{n^2} t^2} \exp\left[-\nu t \left(q^{n^2} - aq_1^n q_2^n t + \frac{1}{3} a^2 q_1^{n^2} t^2\right)\right] \tag{62}$$

$$P^n = \frac{-2\rho a a_2^n q_1^n q^{n^2}}{\left(q^{n^2} - 2aq_1^n q_2^n t + a^2 q_1^{n^2} t^2\right)^2} \exp\left[-\nu t \left(q^{n^2} - aq_1^n q_2^n t + \frac{1}{3} a^2 q_1^{n^2} t^2\right)\right] \tag{63}$$

$a = dU_1/dx_2$, $q^{n^2} = q_1^{n^2} + q_2^{n^2} + q_3^{n^2}$, and the a_i^n and q_i^n are given in the initial conditions (eqs. (37) and (40)) (with the first set of signs). Mean values are obtained by integrating over all space. For instance,

$$\overline{pu_2} = \sum_{n=1}^{3} \frac{1}{2} P^n U_2^n \tag{64}$$

It is clear from the form of equations (60) and (61) that the solution does not satisfy constant periodic boundary conditions. By omitting the term $-(dU_1/dx_2)x_2 \partial u_1/\partial x_1$ as well as the nonlinear terms in equations (57) and (59), we can, however, obtain a simple analytical pseudo solution that satisfies those conditions:

$$u_2 = \sum_{n=1}^{3} a_2^n \exp\left[\nu t \left(2a \frac{q_1^n q_2^n}{q^{n^2}} - q^{n^2}\right)\right] \cos \vec{q}^n . \vec{x} \tag{65}$$

$$p = - \sum_{n=1}^{3} \frac{2\rho a q_1^n a_2^n}{q^{n^2}} \exp\left[\nu t \left(2a \frac{q_1^n q_2^n}{q^{n^2}} - q^{n^2}\right)\right] \sin \vec{q}^n . \vec{x} \tag{66}$$

This solution is useful for checking the numerical calculations and for study-ing the effect of the term $(dU_1/dx_2)x_2 \partial u_2/\partial x_1$ on the fluctuations.

Velocity fluctuations obtained from linearized solutions (numerical and analytical) were plotted (fig. 14). The presence of small-scale structure in the curves for $(dU_1/dx_2)* = 4434$ and its absence in those for $(dU_1/dx_2)* = 0$ are apparent. The curve for no shear (eq. (50)) decays monotonically to zero when extended. This is in contrast to the nonlinear case in figure 13(a) for no shear, where at least larger fluctuations are present. The linearized curves for $(dU_1/dx_2)* = 4434$ in figure 14 follow closely the nonlinear ones in figure 13(b) for short times. Likewise the linearized curves in figure 14 for periodic boundary conditions follow closely those for unbounded conditions for short times. For longer times the fluctuations for unbounded conditions continue to decay, whereas those for constant periodic

boundary conditions grow. Small-scale structure in the curves for unbounded conditions is produced by the term $aq_1^n t x_2$ in the argument of the cosine in equation (60) $(a = dU1/dx2)$. This term arises from the term $-ax_2 \, \partial u_2/\partial x_1$ in equation (57), as is evident from its absence in equation (65), where the term $-ax_2 \, \partial u_2/\partial x_1$ has been neglected.

For discussing the linearized case for constant periodic boundary conditions, it is convenient to convert equations (57) and (59) to a spectral form by taking their three-dimensional Fourier transforms. This gives, for u_2, on neglecting nonlinear terms

$$\frac{\partial \varphi_2^n}{\partial t} = aq_1^n \sum_{\kappa_2'} \frac{1}{\kappa_2'} \varphi_2^n(\kappa_1, \kappa_2 - \kappa_2', \kappa_3) - \nu\left(q_1^{n^2} + \kappa_2^2 + q_3^{n^2}\right)\varphi_2^n$$

$$+ \frac{2aq_1^n \kappa_2 \varphi_2^n}{q_1^{n^2} + \kappa_2^2 + q_3^{n^2}} \qquad (67)$$

where

$$\varphi_2^n(\vec{\kappa}) = \frac{1}{8\pi^3} \int_{-\pi}^{\pi} dx_2 \iint_{-\infty}^{\infty} u_2^n(\vec{x}) e^{-i\vec{\kappa}.\vec{x}} \, dx_1 \, dx_3 \qquad (68)$$

or

$$u_2^n(\vec{x}) = \sum_{\kappa_2=-\infty}^{\infty} \iint_{-\infty}^{\infty} \varphi_2^n(\vec{\kappa}) e^{i\vec{\kappa}.\vec{x}} \, d\kappa_1 \, d\kappa_3 \qquad (68a)$$

$$u_2 = \sum_{n=-3}^{3} u_2^n, \quad \varphi_2 = \sum_{n=-3}^{3} \varphi_2^n \qquad (69)$$

$\vec{\kappa}$ is the wave-number vector, and φ_2 is the Fourier transform of u_2. Note that a finite transform is used in the x_2 direction in order to satisfy periodic boundary conditions at $x_2/x_0 = -\pi, \pi$.

Strictly speaking, equation (67) is for a sawtooth mean-velocity profile, whereas the numerical results are for a uniform mean-velocity gradient. Equation (67) should still apply, however, at least for the present discussion purposes to points inside, but not outside, the numerical grid.

For constant periodic boundary conditions for u_1, small-scale structure in the fluctuations or the transfer of energy between wave numbers is

128

produced by the term containing the summation over κ_2' in equation (67). That term is the Fourier transform of $-ax_2\,\partial u_2/\partial x_1$ (eq. 57)). From its form we see that it can produce a complicated inter-wave-number interaction. The quantity φ_2^n at each κ^n interacts with φ_2^n at every other allowable κ_2. A difference between the solutions for unbounded conditions and those for constant periodic conditions is that only fluctuations at integral κ_2 are possible when periodic conditions are imposed, whereas for unbounded conditions fluctuations are possible at all values of κ_2.

Although the linear term $-ax_2\,\partial u_2/\partial x_1$ is effective in producing oscillations, even in the absence of nonlinear effects (fig. 14), the curves lack the random appearance of those in figure 13(b). Evidently, as in the case of no mean gradients (eq. (50)), the only way we can have a linear turbulent solution is to put the turbulence in the initial conditions (Deissler, 1961). Both $-ax_2\,\partial u_2/\partial x_1$ and the nonlinear terms in equation (57) are necessary to produce the small-scale turbulence in figure 13(b) from nonrandom initial conditions. The former acts like a chopper that chops the flow into small-scale components. Although the latter also do that, their most visible effect here is to produce randomization. As in the preceding section the randomization might occur as a result of the presence of strange attractors (or, more properly, analogous strange behavior) in the flow, by proliferation of eddies or harmonic components (with the loss of identity of the individual eddies) or by both (see section IV for a discussion of these possibilities).

According to the linearized analytical solution given by equation (60), the manufacture of small-scale fluctuations takes place only in the x_2 direction. Figure 15 shows how this has taken place at a moderate time. Figure 16 is a similar plot for the nonlinear case. The randomizing effect of the nonlinear terms is evident.

For the nonlinear case, $u_2/\left(\overline{u_0^2}\right)^{1/2}$ was also plotted against x_1 (fig. 17). The curves show some development of small-scale structure in the x_1 direction due to the interaction of the directional components in the nonlinear case. For the linearized flows small-scale structure developed only in the x_2 direction.

E. Evolution of mean quantities with shear

1. Cross-correlation coefficients

Cross-correlation coefficients $\overline{u_i u_j}/\left(\overline{u_i^2}\right)^{1/2}\left(\overline{u_j^2}\right)^{1/2}$ ($i \neq j$) are plotted against dimensionless time for the nonlinear case in figure 17. Although $\overline{u_1^2} = \overline{u_2^2} = \overline{u_3^2}$ at $t^* = 0$, the initial cross correlations are not zero but are all positive and equal. However, because of the apparent randomization of the flow $\overline{u_2 u_3}$ and $\overline{u_1 u_3}$ approach zero as time increases. On the other hand, the values of the turbulent shear stress $\overline{u_1 u_2}$ change from positive to negative and remain negative because of the dynamics of the imposed mean shear. The presence of the mean-velocity gradient dU_1/dx_2 causes u_1 to be likely

negative when u_2 is positive, so that $\overline{u_1 u_2}$, the correlation between the two, is negative.[2] The waviness in the curves in figure 18, as well as that in some of the curves in later figures (e.g., fig. 21), is probably caused by nonrandom structure in the flow, possibly that produced by the linear term $-(dU_1/dx_2)x_2\,\partial u_1/\partial x_1$ in equation (57) (fig. 14).[10]

2. Growth and anisotropy of the velocity fluctuations

The evolution of the mean-square components of the velocity fluctuations is plotted in figure 19, where $\overline{u_{(i)}^2}^* = (x_0/\nu)^2\,\overline{u_{(i)}^2}$. After an initial adjustment period all of the components increase with time, in agreement with experiment (Harris, et al. (1977) and the numerical results in Rogallo (1981)).

The numerical results in Shaanan, et al. (1975), on the other hand, show $\overline{u_2^2}$ and $\overline{u_3^2}$ decreasing at all times, a difference that remains unexplained. Our $\overline{u_1^2}$ component is the largest of the three, $\overline{u_2^2}$ is the smallest, and $\overline{u_3^2}$ lies slightly above $\overline{u_2^2}$, in agreement with experiment Harris, et al. (1977) and previous numerical results.

3. Accuracy of mean and instantaneous quantities

The effect of discretization error on the numerical results for $\overline{u_2^2}$ is shown in figure 20. Curves are plotted for 16^3, 24^3, and 32^3 grid points, together with a fourth-order extrapolation to zero grid-point spacing (an infinite number of grid points) (Deissler, 1981a, 1981c). The differences between the results for 32^3 points and the fourth-order extrapolation are small but increase somewhat at long times. These results appear to indicate that the numerical results given here for averaged values are reasonably accurate. On the other hand the three-dimensional spatial resolution is probably not great enough (except at early times) to give accurate spatial variations of unaveraged quantities, other than that they have a random appearance. However, since the solutions are hydrodynamically unstable, and extremely sensitive to initial conditions, the actual values of the unaveraged quantities are probably not of great significance.

4. Maintenance of the turbulence

For the case considered in this section (uniform velocity gradient dU_1/dx_2) the one-point correlation equation (14) becomes

$$\frac{\partial}{\partial t}\,\overline{u_i u_j} = -\delta_{i1}\frac{dU_1}{dx_2}\,\overline{u_j u_2} - \delta_{j1}\frac{dU_1}{dx_2}\,\overline{u_1 u_2} + \frac{1}{\rho}\left(\overline{p\frac{\partial u_i}{\partial x_i}} + \overline{p\frac{\partial u_i}{\partial x_j}}\right) - 2\nu\,\overline{\frac{\partial u_i}{\partial x_\ell}\frac{\partial u_i}{\partial x_\ell}} \qquad (70)$$

where derivatives of averaged values with respect to x_i do not appear because averages are taken over a three-dimensional period. This is so even though local inhomogeneities may occur when periodic boundary conditions are used, as discussed earlier.[5]

Figure 21 shows the evolution of pressure-velocity-gradient correlations. (Parts of some of the curves are omitted to avoid confusion.) The pressure-velocity-gradient terms in the one-point correlation equation (eq. (70)), together with the production terms, are responsible for maintaining the turbulence against the dissipation (given by the last term in eq. (70)).

There are no production terms in the equations for $\partial \overline{u_2^2}/\partial t$ and $\partial \overline{u_3^2}/\partial t$

($\delta_{11} \overline{u_j u_2} \, \partial U_1/\partial x_2$ and $\delta_{j1} \overline{u_1 u_2} \, \partial U_1/\partial x_2$ are zero). Thus $\overline{u_2^2}$ and $\overline{u_3^2}$

generally receive energy only from the $\overline{u_1^2}$ component, whose equation has a

nonzero production term. Equation (70) shows that to do that, $\overline{p \, \partial u_j/\partial x_i}$ +

$\overline{p \, \partial u_i/\partial x_j}$ must be positive for $i = j = 2, 3$ and negative for $i = j = 1$.
Figure 21 shows that is actually the case for constant periodic boundary conditions except for an initial adjustment period, so that the turbulence is

maintained (fig. 19). The maintenance of the $\overline{u_2^2}$ or u_2 component is par-

ticularly critical because if u_2 goes to zero, the Reynolds shear stress

$\overline{u_1 u_2}$ in the production term of the $\overline{u_1^2}$ equation (eq. (70)) will go to zero
and there will be nothing to keep the turbulence going. All of the components will then eventually decay. That is what happens in the linearized analysis for unbounded turbulence in figure 21 (see also Deissler, 1961).

The nonlinear results for $\overline{u_2^2}$ are compared with various linearized solu-

tions in figure 22. The same initial conditions are used for all of the cases (eqs. (37) or (38), (40), and (55)). For all of the results, except those for the unbounded linearized case (obtained by using unbounded Fourier transforms

(eq. (60)), the crucial $\overline{u_2^2}$ component eventually increases so that the tur-
bulence or fluctuations are maintained. In the unbounded linearized case

$\overline{u_2^2}$ decreases at all times. That was expected, since the $\overline{u_2^2}$ results for

that case in Deissler (1961, 1970b) (for different initial conditions) decreased at all times. Somewhat unexpected are the linearized results for constant periodic boundary conditions, which show that the fluctuations are maintained for those cases. Whereas figure 21 shows that in the unbounded case the pressure-velocity-gradient correlations remove energy from the

$\overline{u_2^2}$ component and cause the fluctuations to decay as in Deissler (1961, 1970b)

the imposition of constant periodic boundary conditions changes the sign of

those correlations and brings energy into $\overline{u_2^2}$, so that the fluctuations are
maintained. Equation (65), which satisfies periodic boundary conditions, shows that, at least when the term $-(dU_1/dx_2)x_2 \, \partial u_i/\partial x_1$ in equation (57) is

neglected, $\overline{u_2^2}$ increases at large times if $2aq_1^n q_2^n > q^{n^4}$ for at least
one n.

131

5. Spectral transfer terms as stabilizing

Comparing the linearized case for periodic boundary conditions in figure 22 with the corresponding nonlinear case shows that the nonlinear terms have a stabilizing influence. That is, the values of $\overline{u_2^2}$ increase more slowly for the nonlinear case. Moreover comparing the curve for the linearized case with periodic boundary conditions and with the term $-(dU_1/dx_2)x_2\,\partial u_2/\partial x_1$ in equation (57) missing (eq. (65)) with the corresponding curve for that term included shows that the presence of that term also has a stabilizing influence. Since neglect of that term is equivalent to neglecting the mean-gradient transfer term T'_{22} in the spectral equation for $\overline{u_2^2}$ (eq. (26)), we can consider the latter term as stabilizing. Thus both the nonlinear spectral transfer term associated with triple correlations T_{22} and the linear mean-gradient transfer term T'_{22} in the spectral equation (26) for $\overline{u_2^2}$ are stabilizing. The reason is that both terms transfer energy to small eddies, where it is dissipated more easily.

It is of interest that the one-point correlation equation for $\partial\overline{u_i u_j}/\partial t$ (eq. (70)) contains neither a term associated with velocity-gradient transfer nor one associated with nonlinear transfer. That is, both of those processes give zero direct contribution to the rate of change of $\overline{u_i u_j}$: they only change the distribution of energy among the various spectral components or eddy sizes. This spectral transfer, of course, still affects the way in which $\overline{u_i u_j}$ evolves (fig. 22). Even though equation (70) contains no transfer terms, the transfer of energy among the various spectral components of the velocity alters the terms that do appear in equation (70), so that $\partial\overline{u_i u_j}/\partial t$ is affected indirectly. That is not a small effect!

The modified linear pseudosolution given by equations (65) and (66) (dash-dot-dot curve in fig. 21) is the simplest solution in which the fluctuations can be maintained against the dissipation. In obtaining it the only mean-gradient term retained in the equations for u_2 (eqs. (57) and (59), $i = 2$) is $-2(dU_1/dx_2)\partial u_2/\partial x_1$, a source term in the Poisson equation for the pressure. If that term is also neglected, u_2 decays and, as discussed earlier, all of the components of the fluctuations decay. Moreover, as shown in figure 22 and already discussed, the term $-(dU_1/dx_2)x_2\,\partial u_1/\partial x_1$ in equation (57) is stabilizing, so it is of no help in maintaining the fluctuations. Thus, at least in the linearized case, the presence of the source term $-2(dU_1/dx_2)\partial u_2/\partial x_1$ in the Poisson equation for the pressure is necessary for maintaining the fluctuations. That term should play a similar important role in the maintenance of nonlinear turbulence, although in that case it is hard to separate the linear effects from the nonlinear ones. In particular, the role of the nonlinear source term in the Poisson equation for the pressure remains unclear, although it may have an effect similar to that of the linear source term.

F. Return to isotropy

Figures 23 and 24 show the approach to isotropy of nonlinear uniformly sheared turbulence when the shear is suddenly removed. Although the shear produces considerable anisotropy, the components $\overline{u_i^2}$ of the mean-square fluctuation approach equality upon removal of the shear and remain accurately equal. The pressure-velocity-gradient correlations in equation (70) are thus successful in transferring energy among the various directional components in such a way that equality of the $\overline{u_i^2}$ is produced. We note that $\overline{u_2^2}$ continues to increase for a short time after the shear is removed, probably because it receives energy from both $\overline{u_1^2}$ and $\overline{u_3^2}$.

In addition to equality of the $\overline{u_i^2}$, zero cross correlations $\overline{u_i u_j}$ ($i \neq j$) are required for isotropy. Figure 24 shows that $\overline{u_1 u_2}$, which is nonzero when the turbulence is sheared, approaches zero when the shear is removed, and along with the other cross correlations, remains close to zero. The destruction of $\overline{u_1 u_2}$, apparently by nonlinear randomization effects, occurs over a finite time rather than instantaneously on removal of the shear.

Another expected effect of removal of the mean shear is that the small-scale structure produced by the chopping term $-(dU_1/dx_2)x_2 \, \partial u_1/\partial x_1$ in equation (57) should die out. According to figure 25, that occurs almost immediately when dU_1/dx_2 goes to zero, evidently because of the large fluctuating shear stresses between the small-scale eddies. Figure 25 shows, in a particularly graphic manner, the effectiveness of the mean-gradient chopping term in equation (57) in producing small-scale turbulent structure.

VI. INHOMOGENEOUS FLUCTUATIONS AND TURBULENCE (DEVELOPING SHEAR LAYER)

Here, the work is extended to an inherently inhomogeneous developing shear layer so that net diffusion, as well as other turbulence processes, can be considered. This case is general enough to include all of the dynamical processes that ordinarily occur in incompressible turbulence.

For the initial conditions we use a three-dimensional cosine velocity fluctuation, as before, and a mean-velocity profile with a step. Thus, in equation (38) we set

$$U_i = \pi \delta_{i1} V[\text{sgn}(x_2^* - \pi) + 1] \tag{71}$$

where V is a constant with the dimensions of a velocity. Equation (71) is plotted against x_2/x_0 in the curve for $t = 0$ in figure 26, where $V^* = Vx_0/v$, and x_0 is again the initial length scale of the disturbance. For the coefficients given by equation (40) we choose the second set of signs. With this choice of signs $\overline{u_1 u_2}$ does not have to change sign as a result of the dynamics of the flow, as it did in the last section, and the initial

adjustment period is eliminated or greatly shortened. If the longer adjustment period remained, much of the development of the shear layer would be distorted.

In carrying out the numerical solution of equations (1) and (3) we use boundary conditions (44) and (47), where we let

$$(U_1)_{x_j^* = 2\pi + b_j^*} - (U_1)_{x_j^* = b_j^*} = 2\pi \delta_{i1} \delta_{j2} V \qquad (72)$$

Equations (1) and (3) are written in terms of the total velocity $\tilde{u}_i$, but we can calculate the fluctuating part from equation (4), which, for the present case, is $u_i = \tilde{u}_i - \delta_{i1} U_1$, where U_1 is obtained by averaging $\tilde{u}_i$ over x_1 and x_3 for fixed values of x_2. The fluctuations are inhomogeneous in the x_2 direction, except at $t = 0$.

The calculated evolution of the dimensionless mean velocity $U_1^* = (x_0/v)U_1$ (U_2 and U_3 are zero) is plotted against $x_2/x_0 = x_2^*$ for a particular value of $V^* = Vx_0/v$ in figure 26. The results in this section may not be as accurate as those in the previous sections because of the presence of the discontinuity in the initial velocity profile, but they should be qualitatively correct. The shear layer grows (from essentially zero initial thickness) because of the presence of the turbulent and viscous shear stresses. The ratio of turbulent to viscous shear stress (averaged over x_1 and x_3 at the central plane $x_2^* = \pi$) is plotted against dimensionless time in figure 27. Except at early times the growth of the shear layer is almost completely dominated by the turbulent shear stress.

Figure 28 shows the evolution of the instantaneous velocity component u_2 and of the root-mean-square value of u_2 (averaged over the central plane $x_2^* = \pi$). Although the initial conditions are nonrandom, the evolution of u_2 has a random appearance, as in the preceding sections.

On the other hand, $\left(\overline{u_2^2}\right)^{1/2}$ evolves smoothly. These characteristics are again representative of a turbulent flow. The quantity $\left(\overline{u_2^2}\right)^{1/2}$ increases monotonically at small times in contrast to the corresponding curve in section V, where an initial adjustment period was present. As mentioned earlier, the initial adjustment period has been eliminated here by using the second set of signs in equation (40), so that $\overline{u_1 u_2}$ does not have to change sign as a result of the dynamics of the turbulence. The decrease in $\left(\overline{u_2^2}\right)^{1/2}$ near the end of the curve is caused by a decrease in mean-velocity gradient, and thus of turbulence production, at large times (fig. 26).

As in the case in the preceding section, small-scale fluctuations are generated in the inhomogeneous turbulence in figure 28 by the interaction of the mean velocity with the turbulence. This can be seen by comparing figure 28 with figures 1 and 13(a), where mean-velocity gradients are absent. One might expect this since it has been shown (Deissler, 1981b) that, even for a general inhomogeneous turbulence, a term in the two-point spectral equation for the turbulence can transfer energy between scales of motion as a result of the presence of mean gradients.

134

A. Inhomogeneous growth of turbulent energy

A dimensionless plot of turbulent kinetic energy as a function of x_2* and time is given in figure 29, where $\overline{u_k u_k}* = (x_0/\nu)^2 \overline{u_k u_k}$. As for all of the averaged values in this section, $\overline{u_k u_k}/2$ is averaged over x_1 and x_3 for fixed values of x_2. As time increases, an intense concentration of turbulent energy develops near the plane $x_2/x_0 = \pi$, where the mean-velocity gradient is initially infinite. The turbulence is highly inhomogeneous. Inhomogeneity, in fact, seems to be the dominant characteristic of the turbulence generated in the shear layer. The indicated increase in turbulence with time is similar to that obtained experimentally (Brinich, et al., 1975).

B. Turbulence processes in shear layer

Terms in the one-point correlation equation for the rate of change of the turbulent kinetic energy (eq. (15)), which, for the present case, becomes

$$\frac{\partial}{\partial t}\left(\frac{\overline{u_k u_k}}{2}\right) = -\overline{u_1 u_2}\frac{dU_1}{dx_2} - \frac{1}{\rho}\frac{\partial}{\partial x_2}\overline{pu_2} - \frac{\partial}{\partial x_2}\left(\frac{\overline{u_k u_k}}{2}u_2\right)$$

$$+ \nu\frac{\partial^2}{\partial x_2^2}\left(\frac{\overline{u_k u_k}}{2}\right) - \nu\overline{\frac{\partial u_k}{\partial x_\ell}\frac{\partial u_k}{\partial x_\ell}} \tag{73}$$

are plotted for $t* = 0.000293$ in figure 30. As usual, an asterisk on a quantity indicates that it has been nondimensionalized by using x_0 and ν. For instance $(\overline{u_1 u_2}\,dU_1/dx_2)* = (x_0^4/\nu^3)\,\overline{u_1 u_2}\,dU_1/dx_2$. The terms that contribute most to the rate of change of $\overline{u_k u_k}/2$ are the production term $-\overline{u_1 u_2}\,dU_1/dx_2$, the pressure diffusion term $(-\partial \overline{pu_2}/\partial x_2)/\rho$ and the kinetic energy diffusion term $-(1/2)\partial\overline{u_k u_k u_2}/\partial x_2$. The viscous diffusion term $\nu\partial^2(\overline{u_k u_k}/2)/\partial x_2^2$ and the dissipation term $-\nu\overline{\partial u_k/\partial x_\ell\,\partial u_k/\partial x_\ell}$ are small in figure 30. At early times, however, when the mean-velocity gradient is large, the dissipation term is appreciable.

The production term, whose form shows that turbulent energy is produced by work done on the Reynolds shear stress by the mean-velocity gradient, is largest near the plane $x_2* = \pi$, where the velocity gradient is initially infinite. The plots of the pressure and kinetic energy diffusion terms show that those terms are negative near $x_2 = \pi$ and positive away from that plane. Thus, they remove turbulent energy from the maximum-energy region and deposit it where the energy is lower. Both diffusion terms therefore tend to make the turbulence more homogeneous.

A comparison of the turbulence diffusion processes with the spectral transfer processes and the directional transfer processes arising from the

135

pressure-velocity correlations (sections IV and V) is instructive. The spectral transfer processes remove energy from wave-number (or eddy size) regions, where the energy is high, and deposit it in regions of lower energy. The directional transfer processes remove energy from high-energy directional components and deposit it in a directional component (or components) where the energy is lower. The turbulence diffusion processes, as shown here, remove energy from regions of space where the energy is high and deposit it in regions of lower energy. The spectral transfer, directional transfer, and turbulence diffusion processes tend, respectively, to make the turbulence more uniform in wave-number space and more isotropic and homogeneous in physical space.

Although one might suppose that turbulence diffusion terms would always tend to make the turbulence more homogeneous, that supposition is not supported by all of the experimental data. For instance, measurements of wall-bounded turbulence (Laufer, 1954) indicate that the pressure diffusion and the kinetic energy diffusion terms transfer energy in opposite directions, although the total diffusion is from regions of high to regions of lower energy. On the other hand, measurements of turbulence in a free jet (Wygnanski and Fiedler, 1969) and in a wake (Townsend, 1949), which are closer to the case considered here, seem to support the present findings.

VII. A STEADY-STATE HOMOGENEOUS TURBULENCE WITH A SPATIALLY PERIODIC BODY FORCE

In all of the cases considered so far the turbulence either ultimately died out or increased in intensity with time. However, there are many important cases in which the turbulence, after some time, reaches a statistically steady state (e.g., flow in a pipe far from the entrance). Moreover, a discussion of strange attractors (e.g., Eckmann, 1981, and Ott, 1981) should, strictly speaking, be based on a steady-state turbulence; a strange attractor is, roughly, the region of phase space inhabited by the phase point of a system after the initial transients have died out, where the phase point moves in an apparently chaotic fashion. For the decaying turbulence of section IV the attractor would then be only a point in phase space. Of course, we could still talk about analogous strange behavior, even in an unsteady-state case, as we did in section IV-D.

One way of obtaining a statistically steady-state turbulence is by adding a spatially periodic body-force term (forcing term) F_i to the right side of equation (41). A convenient term for that purpose is

$$F_i = -c \left(-\frac{\partial(\tilde{u}_i \tilde{u}_k)}{\partial x_k} - \frac{1}{\rho}\frac{\partial \tilde{p}}{\partial x_i} + v\frac{\partial^2 \tilde{u}_i}{\partial x_k \partial x_k} \right)_0 \tag{74}$$

where the subscript 0 signifies initial values, the $\tilde{u}_i$ are given by equations (38) and (40) with $U_i = 0$ and $\tilde{p}$ by equation (3), and c is a constant. The first set of signs is used in equation (40). Equation (74), which is time independent, is used for F_i at all times. For $c = 1$, the the quantities $\tilde{u}_i$ and $\tilde{p}$, as calculated from equation (1) (with F_i added to the right side) and equation (3), do not change from their initial equation (3), do not change from their initial values. To introduce some initial time

136

dependence, we set $c = 1.05$. The boundary conditions are taken to be periodic, as in section IV.

Calculated results for this case are plotted in figures 31 and 32, where t^* is again equal to $(v/x_0^2)t$ and x_0 is the initial length scale. Figure 31 shows the time evolution of $\tilde{u}_1$ and $\left(\overline{\tilde{u}_1^2}\right)^{1/2}$ at a point away from the center of the numerical grid, where as before, overbars indicate space averages. The values are normalized by dividing them by $\left(\overline{u_0^2}\right)^{1/2}$, the initial value of $\left(\overline{\tilde{u}_1^2}\right)^{1/2} = \left(\overline{\tilde{u}_2^2}\right)^{1/2} = \left(\overline{\tilde{u}_3^2}\right)^{1/2}$. Since we are interested in steady-state solutions at long times it is necessary, to obtain reasonably accurate results, to use a lower Reynolds number than in the preceding cases, where shorter-time transient flows were considered.

Figure 30 shows that, for $0 < t^* < 0.17$, the flow is essentially laminar with small fluctuations of u_1. Then for $0.17 < t^* < 0.18$ there is a rather sharp transition from laminar to turbulent flow, as $\left(\overline{\tilde{u}_1^2}\right)^{1/2}$ increases. For $t^* > 0.18$ the turbulence is statistically steady state, as indicated by the nearly constant value of $\left(\overline{\tilde{u}_1^2}\right)^{1/2}$. Curves for $\tilde{u}_2$ and $\tilde{u}_3$ are similar to those for $\tilde{u}_1$, including the same location of the transition region and nearly the same values for $\left(\overline{\tilde{u}_2^2}\right)^{1/2}$ and $\left(\overline{\tilde{u}_3^2}\right)^{1/2}$ as for $\left(\overline{\tilde{u}_1^2}\right)^{1/2}$.

After the transition region ($t^* > 0.18$) the flow appears to lie on a strange attractor, since it has the following characteristics:[14] first, a volume in the phase space of our system decreases with time, since the Navier-Stokes equations describe a dissipative system and phase-volume shrinkage can be shown to occur for the Navier-Stokes equations.[14] This implies that an attractor exists for our system. Second, the chaotic appearance of the velocity components (figs. 31 and 32) indicates that the attractor is strange. Finally, the fact that transients have died out for $t^* > 0.18$, leaving a statistically steady state (fig. 31), indicates that beyond the transition region the phase point is on the strange attractor.

Figure 32 shows the projection on the $\tilde{u}_2$-$\tilde{u}_3$ plane (at the center of the numerical grid) of the trajectory of the phase point as it moves on the strange attractor. As in figure 6 the trajectory consists of loops and cusps with frequent changes in the sign of the curvature, but unlike figure 6 the trajectory does not, of course, tend toward a point. The cusps might be considered as loops with very small or zero radii. Also, as in figure 6, randomization is very likely associated with the large number of harmonics (eddy sizes) present, as well as with the strange attractor or strange behavior.

---

[14]These characteristics, as well as the possibility of obtaining a steady-state turbulence with periodic boundary conditions by slightly modifying the existing program, were pointed out to the author by R.J. Deissler.

VIII. CONCLUSIONS.

From the present review it is concluded that the nonlinear and linear processes in turbulence can be profitably studied numerically. The results show that, at least at higher Reynolds numbers, an apparently random turbulence can develop from nonrandom initial conditions. The numerically calculated turbulence is not numerical hash, since a large number of time steps correspond to each fluctuation. For both sheared and unsheared fluctuations the structure of the Navier-Stokes equations is such that turbulence can develop even when the/initial flow is nonturbulent. This is indicated by the appearance of the instantaneous velocity fluctuations and by the sensitivity of those fluctuations (and the insensitivity of average values) to small perturbations in the instantaneous initial conditions. The randomness appears to increase as the numerical mesh size decreases. Moreover, the two-time velocity correlation becomes small as the time between the occurrence of the two velocities increases. In addition, for no mean shear the correlation between any two components of the velocity becomes small as the time increases, as a result of the randomization. This correlation is not small initially, even though the three components of the mean-square velocity fluctuation are equal at early as well as at late times for the initial conditions chosen. Also, calculated velocity-derivative skewness factors for no mean shear appear to be of reasonable magnitude when compared with those for isotropic turbulence. Thus, except in the initial period the results for no mean shear evidently give a reasonably good approximation to isotropic turbulence.

The source of the observed randomness may lie in the presence of strange attractors or, more properly, of analogous strange behavior (Monin, 1978) in the phase space of the system, as well as in the occurrence of a large number of eddies or harmonic components (large number of degrees of freedom). It appears that no conclusions can be drawn as to the relative importance of the two processes, but both probably occur. (A strange attractor is a region in the phase space of the system to which solutions are attracted and in which the phase point moves in an apparently chaotic fashion. It can occur even with a small number of degrees of freedom.) Roundoff errors appear not to be a sustaining cause of the randomness; a large decrease in roundoff errors did not appreciably affect the turbulence level or the randomness of the fluctuations, although the instantaneous values were different. Thus, the affect of a large decrease in roundoff errors is similar to that of a small perturbation of the initial conditions. Roundoff errors may in some cases affect the transition to turbulence. The present turbulent solutions bear some similarity to those for low-order models in that both have trajectories in phase space that consist of loops and cusps, with frequent changes in the sign of the curvature of the trajectory (fig. 6). Moreover, with the results from the low-order models in which apparent randomness appears with as few as three degrees of freedom (e.g., in the Lorenz equations), the turbulence observed to be manufactured by the Navier-Stokes equations should perhaps not come as a surprise.

At early times the calculated nonlinear transfer of energy from big eddies to small ones is almost completely dominant and causes a sharp decrease in the size of the microscale. This has not been generally observed experimentally or analytically because the period usually studied is for later times, where the annihilation of small eddies by viscous action causes the scale to grow, even though energy is being transferred to smaller eddies. This later period of scale growth is also observed in the present results.

The nonlinear terms in the equations of motion, besides transferring energy among eddy sizes and producing randomization, are very effective vorticity generators and increase the dissipation and the rate of decay. The increased rate of decay is a result of the nonlinear transfer of energy to smaller eddies; the small eddies decay faster than the big ones because of the higher shear stresses between the small eddies. Calculation of (averaged) terms from unaveraged equations of motion shows, as might be expected, that the flow is dominated by nonlinear inertial effects at early times and by viscous effects at later times (fig. 12). The nonlinear effects are associated with both velocity and pressure terms in the unaveraged equations of motion, even for isotropic turbulence. Since the one- and two-point averaged or correlation equations for isotropic turbulence do not contain pressure terms, the effects of pressure observed for the unaveraged equations must be contained in higher order averaged equations. The infinite hierarchy of averaged equations should contain all effects, as do the unaveraged equations. The only physical processes associated with pressure (that we know about) are interdirectional transfer and spatial diffusion of turbulence (eq. (14)). It thus seems reasonable to attribute the observed pressure effects in the unaveraged equations to those processes. Even though there is no net interdirectional transfer or spatial diffusion in isotropic turbulence, those processes can still be locally operative.

The processes occurring in isotropic turbulence thus include the following: nonlinear randomization, nonlinear spectral transfer (mainly to smaller scales of motion), zero net (but not zero) spatial diffusion and transfer of turbulence among directional components, generation of vorticity or swirl, and viscous dissipation.

If a uniform shear is present in the flow, we have, in addition to these processes, production of turbulence by the mean-velocity gradient, net transfer of turbulence among directional components by pressure forces, and linear spectral transfer among scales of motion by the mean gradient. The last of these processes results in the production of small-scale fluctuations in the flow. This can be attributed to a mean-gradient transfer term in the spectral equation for the velocity fluctuations (eq. (26)). Although we first discussed that term over two decades ago, the recent numerical results considered herein give the first graphic demonstration of the effectiveness of that term in generating a small-scale structure in the turbulence. However, the small-scale fluctuations produced by that term alone (linear solution) are essentially nonrandom. Evidently, the only way we can have a turbulent linear solution, either with or without mean gradients, is to put the turbulence in the initial conditions. To produce the small-scale turbulence from nonrandom initial conditions observed herein for shear flow, the presence of both the linear mean-gradient transfer term and the nonlinear terms in the equations is necessary. The former term, or its equivalent in the unaveraged equation (57), acts like a chopper that chops the flow into small-scale components. The latter terms, while they also produce small-scale components, act most visibly here as randomizers.

In all of the uniform-shear cases calculated with constant periodic boundary conditions, including both linear and nonlinear flows, the pressure-velocity-gradient correlations are successful in distributing energy among the directional components, so that the turbulence or the fluctuations are maintained. This is in spite of the presence of a production term in the equation for only one of the components. Both the linear mean-gradient transfer term

and the nonlinear terms mentioned in the preceding paragraph have a stabilizing effect. That is, they cause the fluctuations to increase at a slower rate. The reason is that both terms transfer energy to small eddies, where it is dissipated more easily. It is shown that, at least for the linearized solution with constant periodic boundary conditions, a mean-gradient source term in the Poisson equation for the pressure is necessary for maintaining the fluctuations against the dissipation. That term should play a similar important role in the maintenance of nonlinear turbulence, although in that case it is hard to separate the linear effects from the nonlinear ones. For the linearized unbounded solution (obtained by using unbounded Fourier transforms) the fluctuations decay, as expected from earlier results.

When the mean-velocity gradient is suddenly removed, the turbulent shear stress goes to zero in a finite time, and the velocity-pressure-gradient correlations cause the turbulence to attain the isotropic state. The intensities of the directional components become and remain equal. In addition, the small-scale structure produced by the mean-gradient transfer term quickly vanishes (fig. 25). Figure 25 shows, in a particularly graphic manner, the effectiveness of the mean-gradient chopping term in equation (57) in producing small-scale turbulent structure.

For a developing shear layer the turbulence is inhomogeneous and, in addition to the processes considered so far, a net spatial diffusion of turbulence occurs. The thickness of the shear layer, which is initially zero, increases with time because of the presence of turbulent and viscous shear stresses. Except at very early times the growth of the shear layer is almost completely dominated by the turbulent shear stress. As time increases, an intense concentration of turbulent energy develops near the plane where the mean-velocity gradient is initially infinite. The turbulence is highly inhomogeneous. The calculated turbulence production is always positive, and is largest near the plane where the velocity gradient is initially infinite. The pressure and the kinetic energy diffusion are negative near that plane and positive away from it. Thus, they remove turbulent energy from the high-energy region and deposit it where the energy is lower. Both diffusion processes therefore tend to make the turbulence more homogeneous.

A comparison of the various transfer and diffusion processes occurring in turbulence is of interest. The spectral transfer processes remove energy from wave-number (or eddy size) regions where the energy is high and deposit it in regions of lower energy. The directional transfer processes remove energy from high-energy directional components and deposit it in a directional component (or components) where the energy is lower. The turbulence diffusion processes remove energy from regions of space where the energy is high and deposit it in regions of lower energy. The spectral transfer, directional transfer, and turbulence diffusion processes tend, respectively, to make the turbulence more uniform in wave-number space and more isotropic and homogeneous in physical space.

By adding a spatially periodic body-force term to the Navier-Stokes equations, a solution is obtained in which the flow first passes through laminar and transition-to-turbulence stages. The turbulence then quickly settles down to a statistically steady state. In this last stage the flow appears to have characteristics corresponding to those of a strange attractor.

REFERENCES

Batchelor, G.K., 1953, <u>Homogeneous Turbulence</u> (Cambridge, New York), pp. 100, 137, 88, 86.

Batchelor, G.K., 1967, <u>An Introduction to Fluid Dynamics</u> (Cambridge, New York), p. 131.

Betchov, R., and A.A. Szewczyk, 1978, Phys. Fluids $\underline{21}$, 871.

Brinich, P.F.; D.R. Boldman, and M.E. Goldstein, 1975, NASA TN D-8034.

Cain, A.B., W.C. Reynolds, and J.H. Ferziger, 1981, Rept. No. SU-TF-14, Stanford Univ.

Ceschino, F., and J. Kuntzmann, 1966, <u>Numerical Solution of Initial Value Problems</u> (Prentice-Hall, Englewood Cliffs, New Jersey), p. 141, example 2, and p. 143.

Champagne, F.H., V.G. Harris, and S. Corrsin, 1970, J. Fluid Mech. $\underline{41}$, 81.

Clark, R.A., J.H. Ferziger, and W.C. Reynolds, 1979, J. Fluid Mech. $\underline{91}$, 1.

Corrsin, S., and W. Kollman, 1977, in <u>Turbulence in Internal Flows</u>, edited by S.N.B. Murthy (Hemisphere, Washington), p. 11.

Deardorff, J.W., 1970, Geophys. Fluid Dyn. $\underline{1}$, 377.

Deissler, R.G., 1958, Phys. Fluids $\underline{1}$, 111.

Deissler, R.G., 1960, Phys. Fluids $\underline{3}$, 176.

Deissler, R.G., 1961, Phys. Fluids $\underline{4}$, 1187.

Deissler, R.G., 1970a, Appl. Sci. Res. $\underline{21}$, 393.

Deissler, R.G., 1970b, Phys. Fluids $\underline{13}$, 1868.

Deissler, R.G., 1972, Phys. Fluids $\underline{15}$, 1918.

Deissler, R.G., 1976, Am. J. Phys. $\underline{44}$, 1128.

Deissler, R.G., 1977, in <u>Handbook of Turbulence, vol. 1</u>, edited by W. Frost and T.H. Moulden (Plenum, New York), p. 165.

Deissler, R.G., 1979, Phys. Fluids $\underline{22}$, 1852.

Deissler, R.G., 1981a, Phys. Fluids $\underline{24}$, 1595.

Deissler, R.G., 1981b, Phys. Fluids $\underline{24}$, 1911.

Deissler, R.G., 1981c, NASA TM-82925.

Deissler, R.G., 1982, NASA TM-82969.

Deissler, R.G.; and B.M. Rosenbaum, 1973, NASA TN D-7284.

Eckmann, J.P., 1981, Rev. Mod. Phys. $\underline{53}$, 643.

Feiereisen, W.J., E. Shirani, J.H. Ferziger, and W.C. Reynolds, 1982, in
   Turbulent Shear Flows 3, edited by L.J.S. Bradbury, F. Durst, B.E.
   Launder, F.W. Schmidt, and J.H. Whitelaw (Springer-Verlag, New York),
   p. 309.

Ferziger, J.H., 1977, AIAA J. $\underline{15}$, 1261.

Franceschini, V., 1983, Phys. Fluids $\underline{26}$, 433.

Frost, W., and T.H. Moulden, 1977, Handbook of Turbulence (Plenum, New York).

Harris, V.G., J.A.H. Graham, and S. Corrsin, 1977, J. Fluid Mech. $\underline{81}$, 657.

Heisenberg, W., 1948, Proc. Roy. Soc. A $\underline{195}$, 402.

Herring, J.R., 1973, in Free Turbulent Shear Flows, Vol. 1 - Conference
   Proceedings, NASA SP-321, p. 41.

Hinze, J.O., 1975, Turbulence (McGraw-Hill, New York).

von Karman, T., 1937a, R. Aeronaut. Soc. J. $\underline{41}$, 1109.

von Karman, T., 1937b, J. Aero. Sci. $\underline{4}$, 131.

Lanford, O.E., 1982, in Annual Review of Fluid Mechanics, vol. 14, edited by
   M. VanDyke, J.V. Wehausen, and J.L. Lumley (Annual Reviews, Palo Alto, CA),
   p. 347.

Laufer, J., 1954, NACA TR-1174.

Ling, S.C., and A. Saad, 1977, Phys. Fluids $\underline{20}$, 1796.

Lorenz, E.N., 1963, J. Atmos. Sci. $\underline{20}$, 130.

McCormick, J.M., and M.G. Salvadore, 1964, Numerical Methods in Fortran

   (Prentice-Hall, Englewood Cliffs, NJ), p. 38.

Moin, P., and J. Kim, 1982, J. Fluid Mech. $\underline{118}$, 341.

Monin, A.S., 1978, Usp. Fiz. Nauk [Sov., Phys. - Usp. $\underline{21}$, 429.

Orszag, S.A., 1977a, in Fluid Dynamics, edited by R. Balian and J.L. Peube
   (Gordon and Breach, New York), pp. 273, 261.

Orszag, S.A., 1977b, in Handbook of Turbulence, edited by W. Frost and
   T.H. Moulden (Plenum, New York), p. 281.

Orszag, S.A., and M. Israeli, 1974, in Annual Review of Fluid Mechanics,
   edited by M. Van Dyke, W.G. Vincenti, and J.V. Wehausen (Annual Reviews
   Inc., Palo Alto, CA), pp. 282-288.

Orszag, S.A., and A.T. Patera, 1981, Phys. Rev. Lett. 47, 832.

Orszag, S.A., and G.S. Patterson, Jr., 1972, Phys. Rev. Lett. 28, 76.

Ott, E., 1981, Rev. Mod. Phys. 53, 655.

Rabinovich, M.I., 1978, Usp. Fiz. Nauk [Sov. Phys. - Usp. 21, 443.

Reynolds, O., 1883, Phil. Trans. Roy. Soc. London 174, 935.

Reynolds, O., 1895, Phil. Trans. Roy. Soc. London 186, 123.

Richardson, L.F., 1922, Weather Prediction by Numerical Process (Cambridge, New York).

Rogallo, R.S., 1981, NASA TM 81315.

Ruelle, D., 1976, in Turbulence and Navier-Stokes Equations, edited by R. Temam (Springer-Verlag, New York), p. 146.

Schumann, U., G. Groetzbach, and L. Kleiser, 1980, in Prediction Methods for Turbulent Flows edited by W. Kollmann (Hemisphere Publishing Comp., Washington, D.C.), p. 123.

Shaanan, S., J.H. Ferziger, and W.C. Reynolds, 1975, Rept. No. SU-TF-6, Stanford Univ.

Siggia, E.D., 1981, J. Fluid Mech. 107, 375.

Smagorinsky, J., 1963, Mon. Weath. Rev. 93, 99.

Taylor, G.I., 1921, Proc. Lond. Math. Soc. 20, 196.

Taylor, G.I., 1935, Proc. Roy. Soc. A, 151, 421.

Taylor, G.I.; and A. E. Green, 1937, Proc. Roy. Soc. A, 158, 499.

Townsend, A.A., 1949, Proc. Roy. Soc. London, 197A, 124.

Uberoi, M.S., 1963, Phys. Fluids 6, 1048.

Van Dyke, M., 1975, SIAM J. Appl. Math. 28, 720.

Wygnanski, I., and H. Fiedler, 1969, J. Fluid Mech. 38, 577.
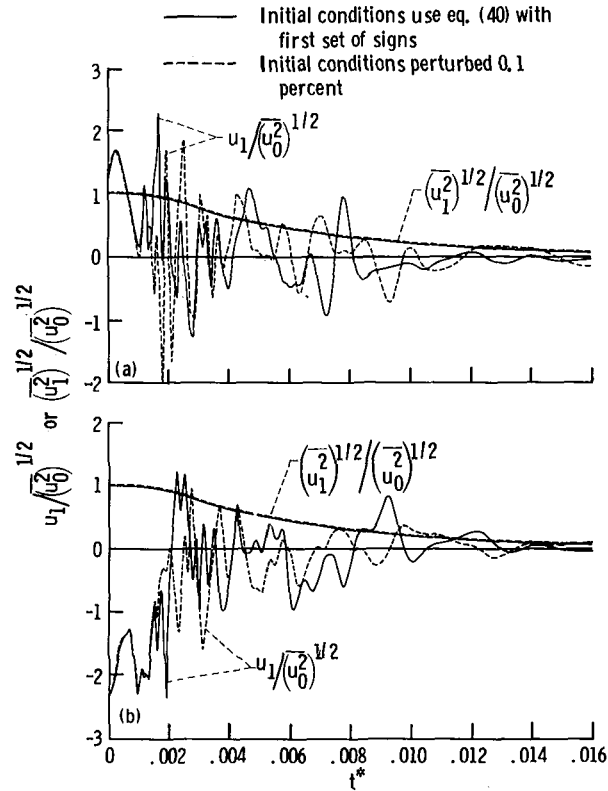
(a) $x_1^* = x_2^* = 9\pi/8$, $x_3^* = 3\pi/8$, for unaveraged fluctuations.

(b) $x_1^* = x_2^* = x_3^* = \pi$, for unaveraged fluctuations.

Figure 1. – Calculated evolution of turbulent velocity fluctuations (normalized by initial condition) for a high Reynolds number $\left(\overline{u_0^2}\right)^{1/2} x_0/\nu = 2217$. No mean shear; root-mean-square fluctuations spatially averaged; 32^3 grid points.

144

(a) 8^3 grid points.
(b) 16^3 grid points.
(c) 32^3 grid points.
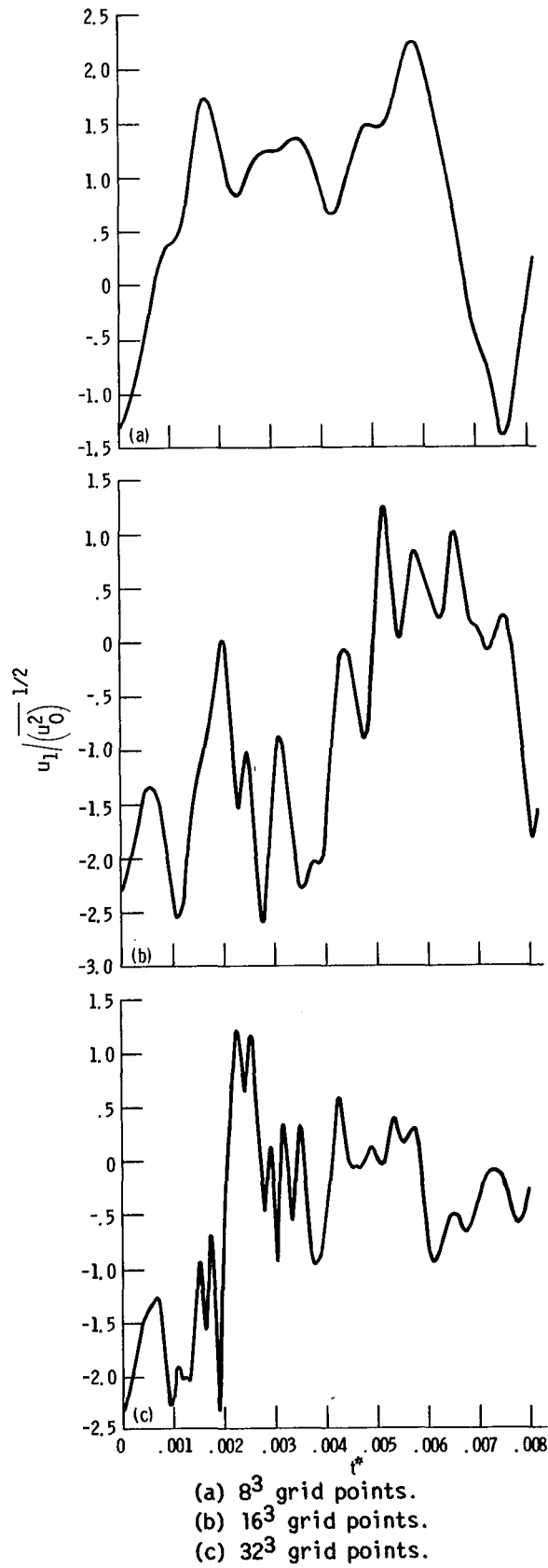
Figure 2. - Effect of numerical mesh size on calculated evolution of velocity fluctuations. No mean shear; $\left(\overline{u_0^2}\right)^{1/2} x_0/\nu = 2217$; $x_i^* = \pi$ (at grid center).

145

(a) $t_0 = 0$.

(b) $t_0 = 0.00813$.
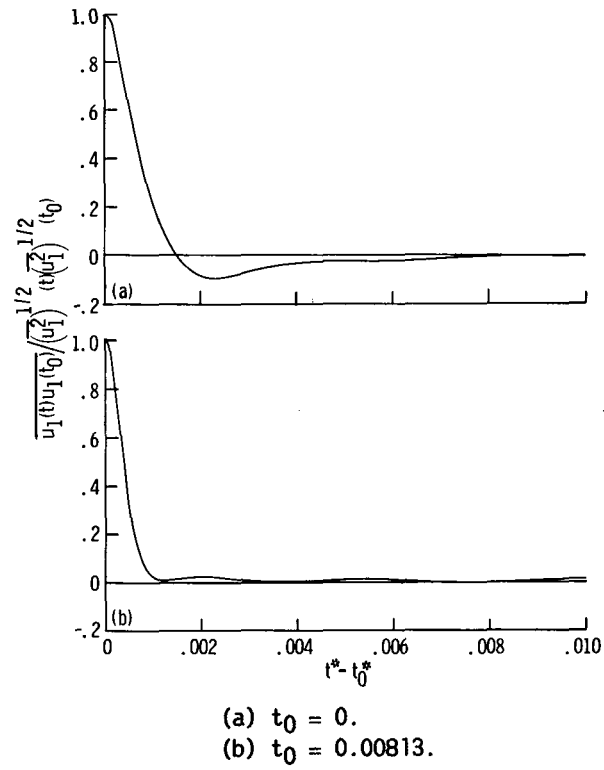
Figure 3. — Calculated correlation coefficient for velocities at dimensionless times t_0^* and t_0^* plotted against $t^* - t^*$. No mean shear; $\left(\overline{u_0^2}\right)^{1/2} x_0/\nu = 2217$; 32^3 grid points.
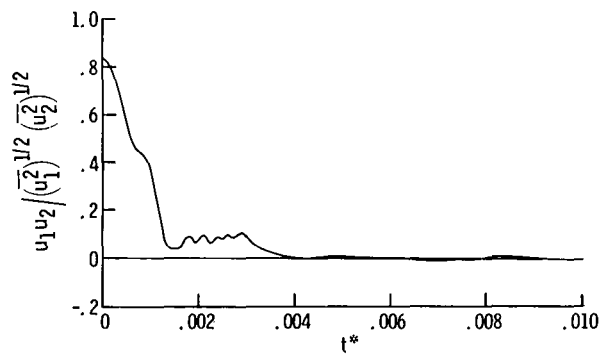
Figure 4. — Calculated correlation coefficient for two velocity components plotted against dimensionless time. No mean shear; $\left(\overline{u_0^2}\right)^{1/2} x_0/\nu = 2217$; 32^3 grid points.

146
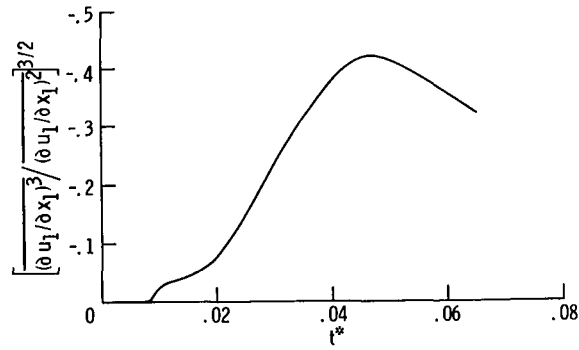
Figure 5. – Calculated evolution of velocity–derivative skewness factor. No mean shear; $\left(\overline{u_0^2}\right)^{1/2} x_0/\nu = 2217$; 32^3 grid points.
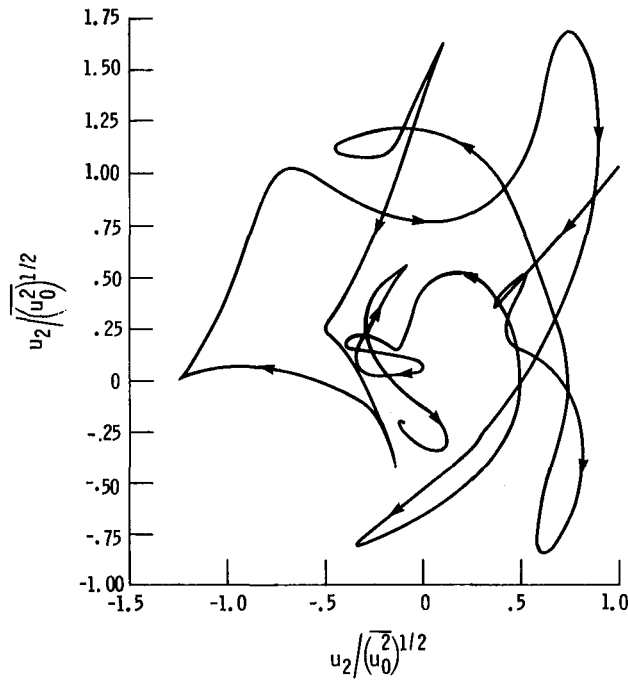
Figure 6. – Calculated trajectory of phase point projected on u_1–u_2 plane $x_1^* = x_2^* = 9\pi/8$, $x_3^* = 3\pi/8$, and $0.00236 < t^* < 0.0108$. Arrows indicate direction of time. No mean shear; 32^3 grid points.
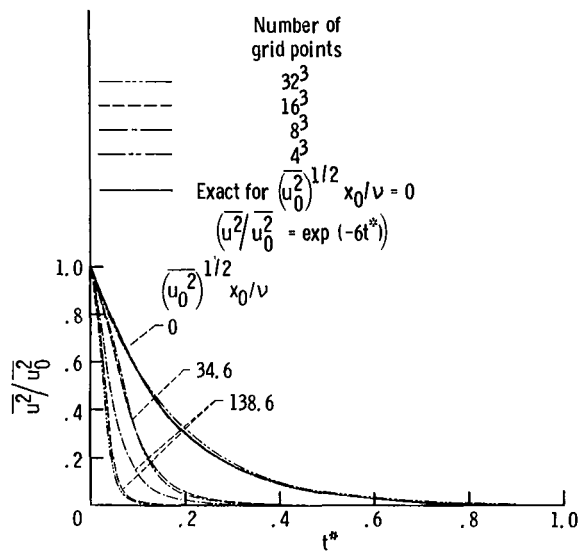
Figure 7. – Effect of numerical mesh size on evolution of $\overline{u^2}$ at low and moderate Reynolds numbers. No mean shear. $\overline{u^2} = \overline{u_1^2} = \overline{u_2^2} = \overline{u_3^2}$.
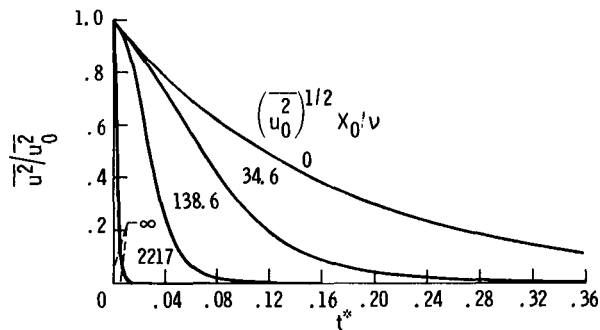
Figure 8. – Calculated evolution of mean-square-velocity fluctuations (normalized by initial value) for various initial Reynolds numbers. No mean shear; $\overline{u^2} = \overline{u_1^2} = \overline{u_2^2} = \overline{u_3^2}$; extrapolated to mesh size.
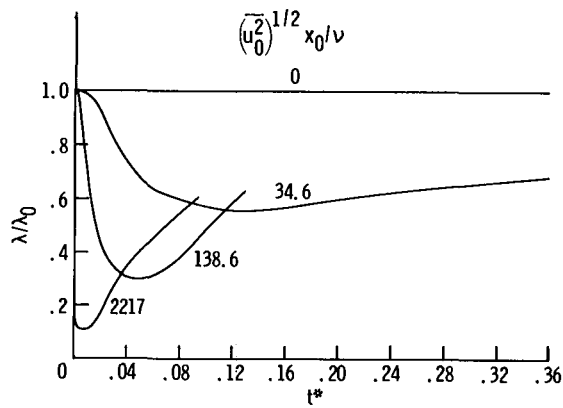
Figure 9. – Calculated evolution of microscale of velocity fluctuations (normalized by initial value) for various initial Reynolds numbers. No mean shear; extrapolated to zero mesh size.
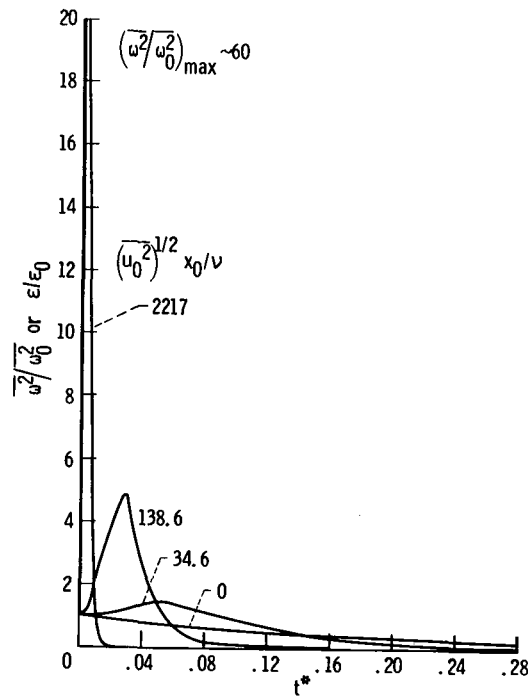
Figure 10. – Calculated development of mean-square-vorticity fluctuations $\overline{\omega}^2$ or dissipation ε (normalized by initial value) for various initial Reynolds numbers. No mean shear; extrapolated to zero mesh size.
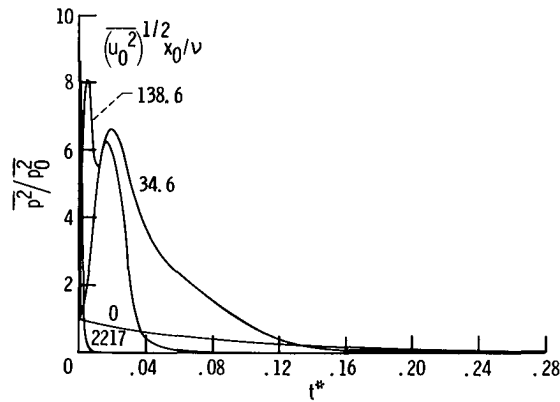
Figure 11. – Calculated evolution of mean–square pressure fluctuation (normalized by initial value) for various initial Reynolds numbers. No mean shear. Extrapolated to zero mesh size.
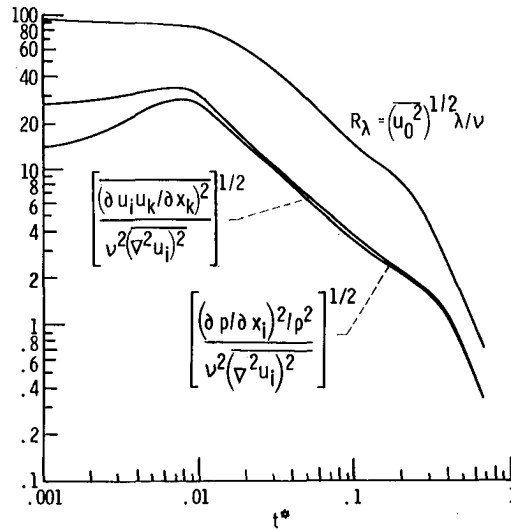
Figure 12. – Three measures of relative importance of inertial and viscous effects plotted against dimensionless time. No mean shear; $\overline{u_0^2}^{1/2} x_0/\nu = 69.3$; i = 1, 2, or 3; extrapolated to zero mesh size.

Initial conditions use eq. (40)
with first set of signs
Initial conditions perturbed
0.1 percent

4

2 $u_2/\left(\overline{u_0^2}\right)^{1/2}$ $\left(\overline{u_2^2}\right)^{1/2}/\left(\overline{u_0^2}\right)^{1/2}$

0

(a)

-2

$u_2/\left(\overline{u_0^2}\right)^{1/2}$ or $\left(\overline{u_2^2}\right)^{1/2}/\left(\overline{u_0^2}\right)^{1/2}$

6

4

2

$u_2/\left(\overline{u_0^2}\right)^{1/2}$ $\left(\overline{u_2^2}\right)^{1/2}/\left(\overline{u_0^2}\right)^{1/2}$

0

-2

-4

(b)

-6
0   .0005   .0010   .0015   .0020   .0025   .0030   .0035   .0040   .0045

t

(a) $(dU_1/dx_2)^* = 0$.

(b) $(dU_1/dx_2)^* = 4434$.
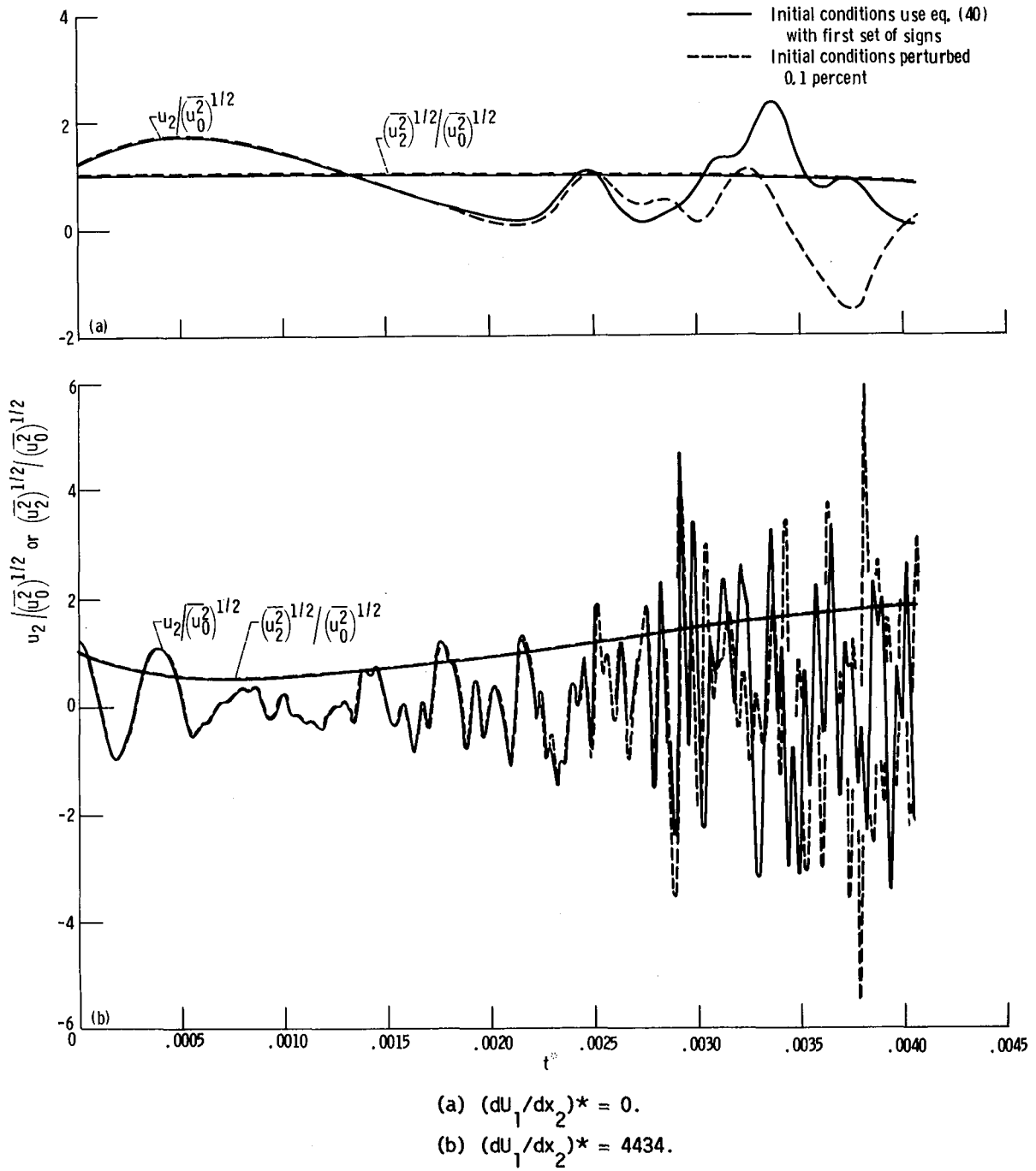
Figure 13. – Effect of uniform shear on calculated evolution of nonlinear turbulent velocity

fluctuations (normalized by initial value) for a high Reynolds number $\left[\left(\overline{u_0^2}\right)^{1/2} x_0/\nu = 1108\right]$.

Root-mean-square fluctuations are spatially averaged; 32^3 grid points; $x_1^* = x_2^* = 9\nu/8$,
$x_3^* = 3\pi/8$ for unaveraged fluctuations.
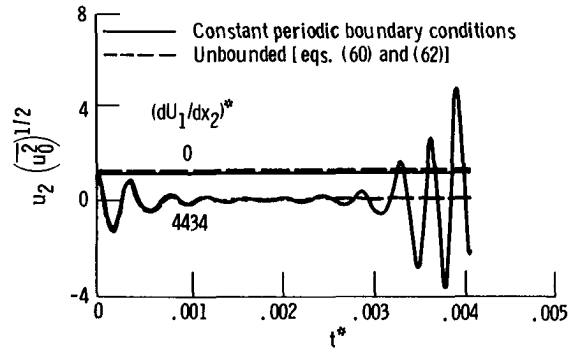
Figure 14. – Calculated evolution of linearized velocity fluctuations (normalized by initial value). $\left(\overline{u_0^2}\right)^{1/2} x_0/\nu = 1108$; $x_1^* = x_2^* = 9\pi/8$; $x_3^* = 3\pi/8$; 32^3 grid points.
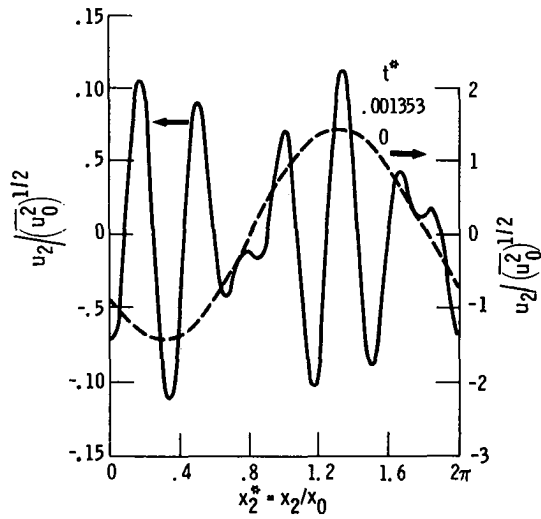
Figure 15. – Linearized analytical solution for $u_2/\left(\overline{u_0^2}\right)^{1/2}$ plotted against x_2^* for unbounded (eq. (60)). $x_1^* = 9\pi/8$; $x_3^* = 3\pi/8$; $(dU_1/dx_2)^* = 4434$; $\left(\overline{u_0^2}\right)^{1/2} x_0/\nu = 1108$.
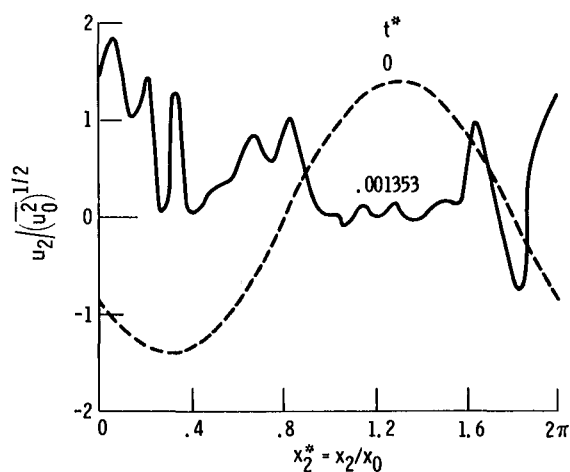
Figure 16. – Nonlinear solution for $u_2/\left(\overline{u_0^2}\right)^{1/2}$ plotted against x_2^*. $x_1^* = 9\pi/8$; $x_3^* = 3\pi/8$; $(dU_1/dx_2)^* = 4434$; $\left(\overline{u_0^2}\right)^{1/2} x_0/\nu = 1108$; 32^3 grid points.
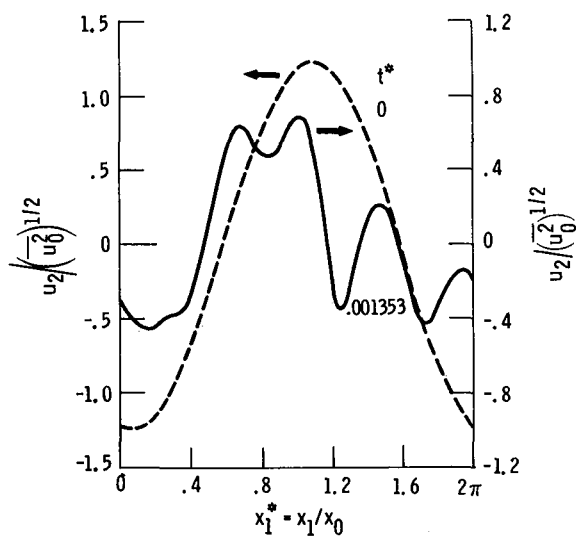
Figure 17. Nonlinear solution for $u_2/\left(\overline{u_0^2}\right)^{1/2}$ plotted against x_1^*. $x_2^* = 9\pi/8$; $x_3^* = 3\pi/8$; $(dU_1/dx_2)^* = 4434$; $\left(\overline{u_0^2}\right)^{1/2} x_0/\nu = 1108$; 32^3 grid points.

153
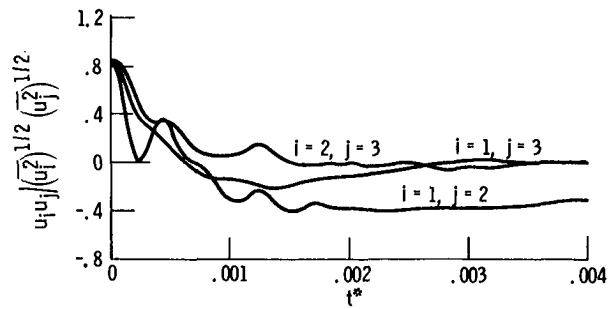
Figure 18. – Calculated cross-correlation coefficients (i ≠ j) plotted against dimensionless time. $(dU_1/dx_2)^* = 4434$; $\overline{u_0^2}^{1/2} x_0/\nu = 1108$; 32^3 grid points.
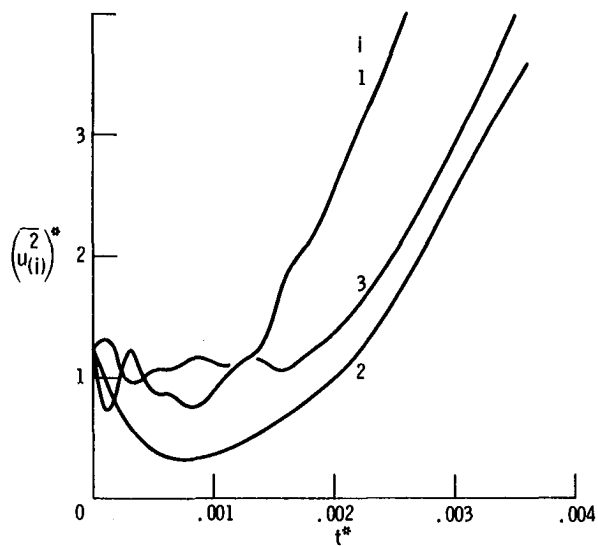
Figure 19. – Calculated evolution of mean-square velocity components. $(dU_1/dx_2)^* = 4434$; $\left(\overline{u_0^{*2}}\right)^{1/2} x_0/\nu = 1108$; 32^3 grid points.
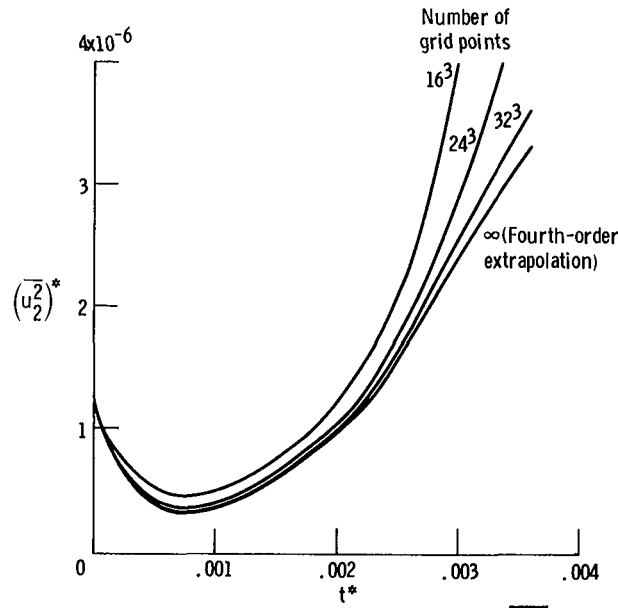
Figure 20. Effect of numerical mesh size on evolution of $\overline{u_2^{2*}}$. $(dU_1/dx_2)^* = 4434$; $\left(\overline{u_0^2}\right)^{1/2} x_0/\nu = 1108$.
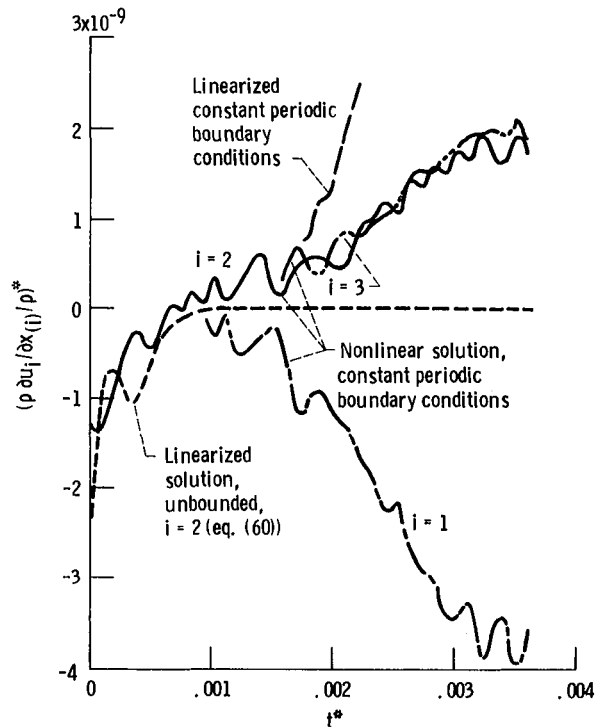
Figure 21. – Calculated evolution of pressure-velocity-gradient correlations. $(dU_1/dx_2)^* = 4434$; $\left(\overline{u_0^2}\right)^{1/2} x_0/\nu = 1108$; 32^3 grid points.
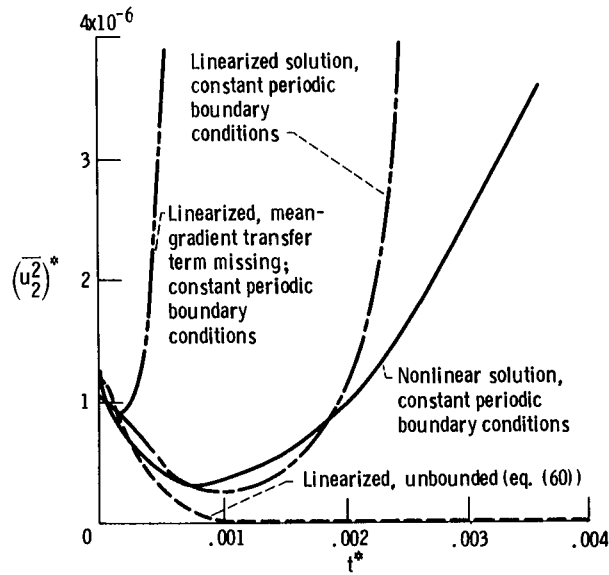
Figure 22. – Evolution of $\overline{u_2^2}$ for various linear and nonlinear solutions. $(dU_1/dx_2)^* = 4434$; $\left(\overline{u_0^2}\right)^{1/2} x_0/\nu = 1108$.
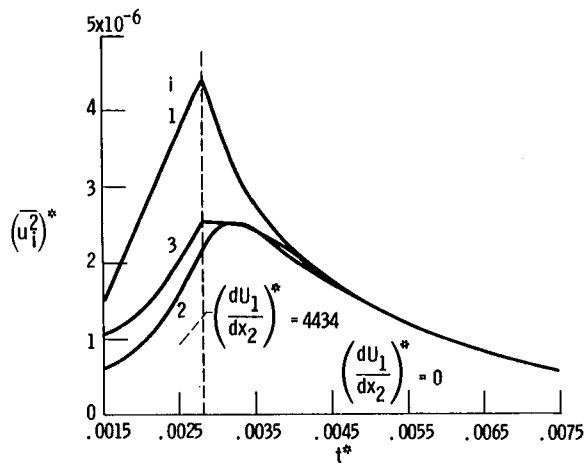
Figure 23. – Calculated approach to isotropy of uniformly sheared turbulence upon sudden removal of the shear. $\left(\overline{u_0^{*2}}\right)^{1/2} x_0/\nu = 1108$; 32^3 grid points.
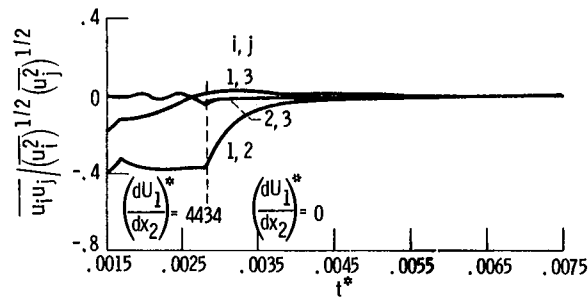
Figure 24. – Calculated evolution of cross-correlation coefficients upon sudden removal of uniform shear. $\left(\overline{u_0^2}\right)^{1/2} x_0/\nu = 1108$; 32^3 grid points.
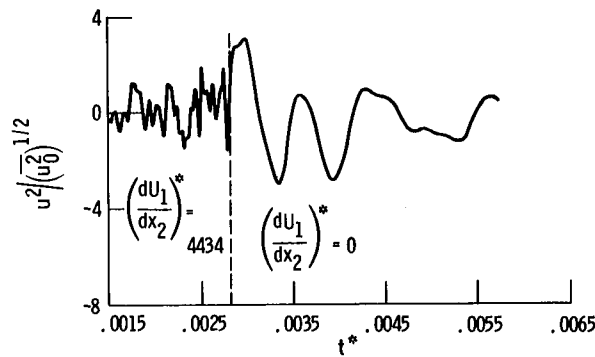
Figure 25. – Effect of removal of uniform shear on structure of turbulence. $\left(\overline{u_0^2}\right)^{1/2} x_0/\pi = 1108$; 32^3 grid points.
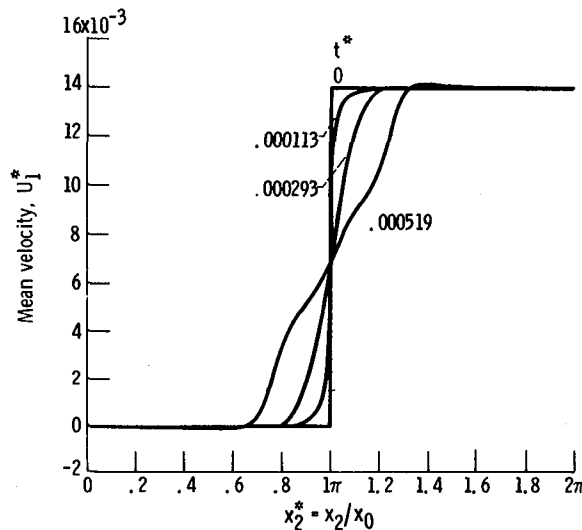
Figure 26. – Calculated development of shear layer mean-velocity profile with dimensionless time. $\left(\overline{u_0^2}\right)^{1/2} x_0/\nu = 554$; $V^* = 2216$ in eq. (71); 32^3 grid points.
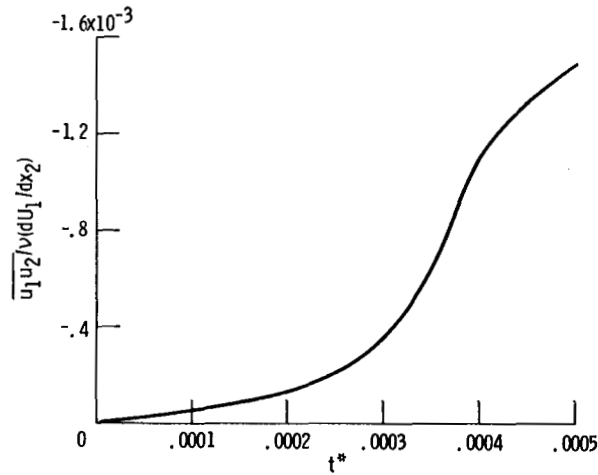
Figure 27. – Calculated time variation of ratio of turbulent-to-viscous shear stress for developing shear layer at $x_2^* = \pi. \left(\dfrac{\overline{u_0^2}}{}\right)^{1/2} x_0/\nu = 554;\ V^* = 2216$ in eq. (71); 32^3 grid points.
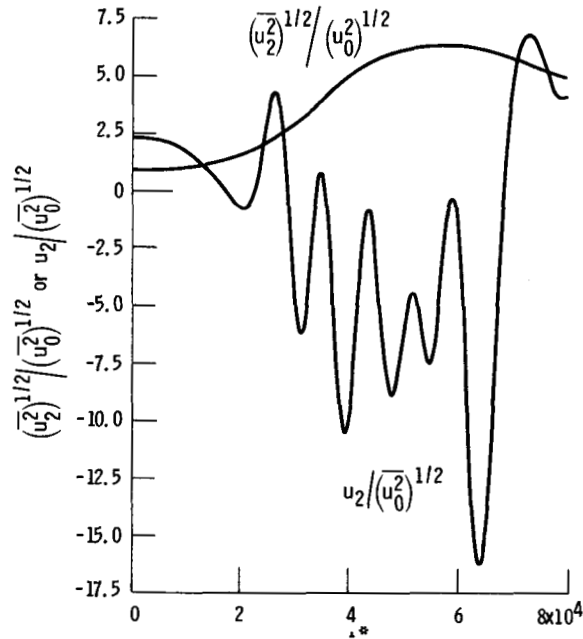

Figure 28. – Calculated evolution of turbulent velocity fluctuations (normalized by initial value) for developing shear layer. Unaveraged fluctuations are calculated at center of numerical grid $(x_1^* = \pi)$. Root-mean-square fluctuations are averaged over x_1^* and x_3^* at central plane $x_2^* = \pi. \left(\dfrac{\overline{u_0^2}}{}\right)^{1/2} x_0/\nu = 554;\ V^* = 2216$ in eq. (71); 32^3 grid points.
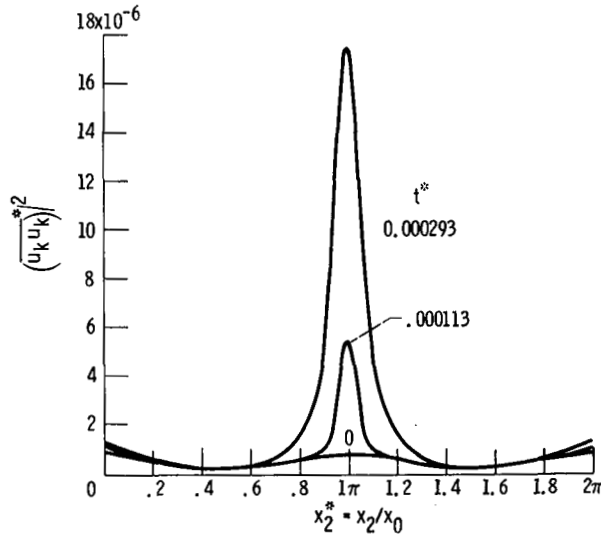
158

Figure 29. – Development of dimensionless kinetic energy profile with dimensionless time for develop-ing shear layer. $\left(\overline{u_0^2}\right)^{1/2}$ $x_0/\nu = 554$; $V^* = 2216$ in eq. (71); 32^3 grid points.
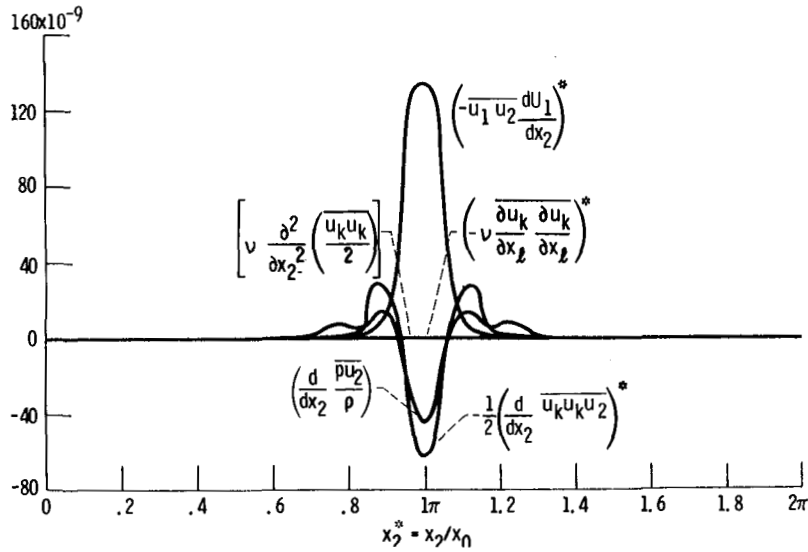

Figure 30. – Plot of terms in one-point correlation equation for kinetic energy (eq. (73)) for devel-oping shear layer. $\left(\overline{u_0^2}\right)^{1/2}$ $x_0/\nu = 554$; $V^* = 2216$ in eq. (71); $t^* = 0.000293$; 32^3 grid points.
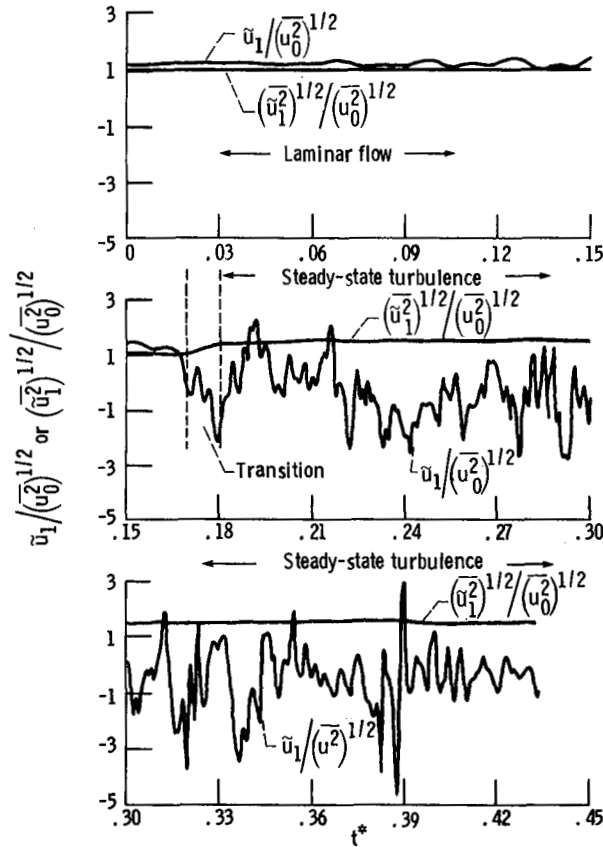
Figure 31. – Calculated evolution of turbulent velocity fluctuations (normalized by initial condition) with a spatially periodic body force. $\left(\overline{u_0^2}\right)^{1/2} x_0/\nu = 138.6$; $x_1^* = x_2^* = 9\pi/8$; $x_3 = 3\pi/8$ for unaveraged fluctuations. Root-mean-square fluctuations spatially averaged; 32^3 grid points.
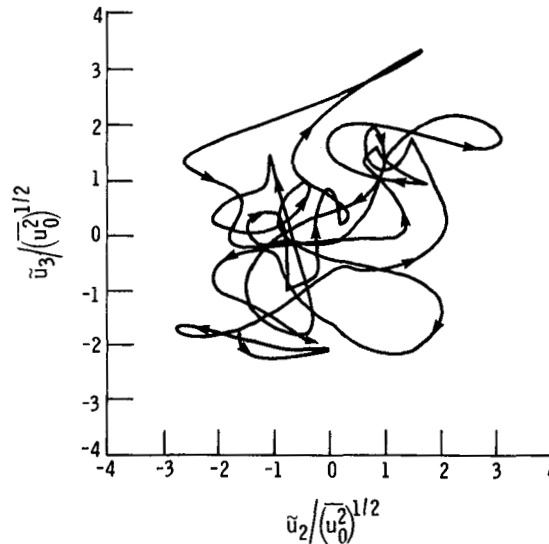

Figure 32. – Calculated trajectory of phase point projected on u_2-u_3 plane at numerical grid center with a spatially periodic body force. $0.26 < t^* < 0.32$; $\left(\overline{u_0^2}\right)^{1/2} x_0/\nu = 138.6$; 32^3 grid points. Arrows indicate direction of time.